Hydrodynamic mechanisms of cell and particle trapping in microfluidics

A. Karimi, S. Yazdi, and A. M. Ardekani

View Online   Export Citation   CrossMark

ARTICLES YOU MAY BE INTERESTED IN

Hydrodynamic mechanisms of cell and particle trapping in microfluidics

A. Karimi,[1] S. Yazdi,[2] and A. M. Ardekani[1,a)]

[1]*Department of Aerospace and Mechanical Engineering, University of Notre Dame, Notre Dame, Indiana 46556, USA*
[2]*Department of Chemical Engineering, The Pennsylvania State University, University Park, Pennsylvania 16802, USA*

Focusing and sorting cells and particles utilizing microfluidic phenomena have been flourishing areas of development in recent years. These processes are largely beneficial in biomedical applications and fundamental studies of cell biology as they provide cost-effective and point-of-care miniaturized diagnostic devices and rare cell enrichment techniques. Due to inherent problems of isolation methods based on the biomarkers and antigens, separation approaches exploiting physical characteristics of cells of interest, such as size, deformability, and electric and magnetic properties, have gained currency in many medical assays. Here, we present an overview of the cell/particle sorting techniques by harnessing intrinsic hydrodynamic effects in microchannels. Our emphasis is on the underlying fluid dynamical mechanisms causing cross stream migration of objects in shear and vortical flows. We also highlight the advantages and drawbacks of each method in terms of throughput, separation efficiency, and cell viability. Finally, we discuss the future research areas for extending the scope of hydrodynamic mechanisms and exploring new physical directions for microfluidic applications. © 2013 American Institute of Physics. [http://dx.doi.org/10.1063/1.4799787]

I. MOTIVATION

Manipulation and sorting of cells and particles suspended in microfluidic platforms raise great interest in biomedical applications, such as oncology,[1] stem cell research,[2] and genomic mapping.[3] Isolating targeted cells from the surrounding environment, e.g., blood sample, is tremendously beneficial in diagnostic and therapeutic operations. In this regard, capturing the least abundant cells plays a vital role in diagnosis of some lethal diseases, such as malaria,[4] cancer,[5] and HIV disease.[6] For example, collecting the circulating tumor cells (CTCs)[7] and fetal cells[8] in peripheral blood is essential for early detection of cancer and parental diagnosis of chromosomal diseases. Moreover, purified cell samples with enhanced concentration of cells of interest provide a rich environment to study the biological and physical properties of those cells.

The non-microfluidic techniques developed for cell separation, such as membrane filtration,[9] centrifugation method,[10] fluorescence activated cell sorting (FACS),[11] and magnetic activated cell sorting (MACS),[12] cover a wide range of applications. However, microfluidic-based devices introduce several advantages, including higher processing rates, lower sample use, enhanced spatial resolution, and increased accessibility due to lower cost.[13] In addition, contrary to the conventional cytometry techniques where their dependence on biochemical labels for cell identification limits their use in some applications, these alternative methods are label-free, i.e., trap cells and particles based on their intrinsic physical characteristics, including size, shape, deformability, density, polarizability, magnetic susceptibility, and so on. Exploiting these properties, the separation is achieved by applying the relevant force fields, such as optical,[14]

---

a)Electronic mail: aardekan@nd.edu.

electric,[15] magnetic,[16] acoustic,[17] and hydrodynamic forces.[18] The controlling mechanism in the aforementioned handling techniques can be classified in two categories: active methods based on the application of external force fields and passive methods where their functionality is established by harnessing microchannel geometrical effects and nonlinear hydrodynamic forces. In the past decade, extensive investigations have been conducted in order to trap and sort cells and particles using either innovative active techniques, such as dielectrophoresis (DEP),[19–22] magnetophoresis,[23] acoustophoresis,[24] and optical tweezers,[25] or novel passive approaches, including pinched flow fractionation (PFF),[26] hydrodynamic filtration,[27] biomimetic methods,[28] hydrophoretic focusing,[29] deterministic lateral displacement (DLD),[30] and surface acoustic wave (SAW)-induced streaming.[31] Each of these methods is associated with some advantages and deficiencies which make them preferable in certain applications. Comprehensive review papers on the focusing and sorting techniques in microfluidics have been authored in recent years which describe the underlying mechanisms and corresponding performance of the aforementioned methods.[13,31–39]

In the current review article, we focus on the basic physics and applications of two families of label-free, passive methods utilized to handle and separate cells and particles by exploiting forces exerted on them due to hydrodynamic effects arising in microfluidic devices. The first approach employs the well-known phenomenon of cross stream migration of suspended particles in confined flows. It has been shown[40] that particles exposed to a shear flow experience a lift force perpendicular to the flow direction where its orientation and strength depend on several factors, including channel geometry, flow rate, rheological properties of the carrier fluid, and physical characteristic of the particle. The second approach utilizes the vortical flow induced by acoustic streaming to trap and sort cells/particles within the vortices. In this scheme, eddies generated by the oscillation of solid or soft boundaries perturb the flow, creating separatrices which segregate particles based on their size and deformability. In the following sections, the physical mechanisms of these methods have been generally described, and a survey of the studies employing these techniques has been presented.

II. HYDRODYNAMICS OF CROSS STREAM MIGRATION

In this section, we address the underlying physics of the lateral migration of the cells and particles engendered by a variety of hydrodynamic forces, and then we describe the pertinent studies harnessing these effects in microfluidic devices for trapping and sorting applications. To quantify the relative importance of the determinant physical phenomena, dimensionless numbers are often used which express where a system lies in fluidic parameter space. These dimensionless groups are summarized in Table I with their mathematical definition and physical interpretation.

A. Inertial effects

Nonlinear effects, such as inertia in laminar flows, result in cross streamline migration of the particles. The relative importance of inertia can be quantified by Reynolds number ($Re = \rho U D_h / \mu$) which describes the ratio of inertial to viscous forces, with ρ, μ, and U being

TABLE I. Dimensionless numbers used in this review.

Re	Reynold number	$\frac{\rho U D_h}{\mu}$	Inertial force/viscous force
Pe	Péclet number	$\frac{\dot{\gamma} a^2}{D}$	Diffusive time scale/convective time scale
κ	Blockage ratio	$\frac{a}{D_h}$	Particle size/channel size
Wi	Weissenberg number	$\lambda_r \dot{\gamma}$	Relaxation time/shear rate time
El	Elasticity number	$\frac{\mu \lambda_r}{\rho D_h^2}$	Elastic force/inertial force
De	Dean number	$Re(\frac{D_h}{2R_c})^{1/2}$	(Centrifugal × inertial forces)$^{1/2}$/viscous force
R_f	Inertial force ratio	$\frac{2R_c a^2}{D_h^3}$	Lift force/Dean drag force

the density, viscosity, and mean velocity of the fluid, respectively, while D_h is the hydraulic diameter of the channel implying the actual diameter in case of a circular tube and equal to $2WH/(W+H)$ for a rectangular channel with width W and height H. It can be shown[41] that in the limit of zero Reynolds number, i.e., Stokes flow, lateral migration of a neutrally buoyant particle suspended in a confined flow of a Newtonian fluid is nonexistent due to linearity and thus reciprocality of the system. But in the flow regime where $Re \gtrsim O(1)$, in addition to the drag force in the axial direction, transverse forces are exerted on the suspended particles compelling them to migrate laterally towards final stable locations, also known as equilibrium positions. This phenomenon was first studied in early experiments of Segré and Silberberg[42–44] where they observed formation of annular aggregates of neutrally buoyant rigid spheres initially dispersed randomly in a pipe flow with $Re \sim O(1-100)$. Constrained by the lateral lift forces, the particles concentrated at a radial position at approximately 0.6 pipe radius, creating the so-called tubular pinch effect.[45] Since this discovery, many analytical,[46–51] experimental,[52–54] and numerical[55–57] investigations have been conducted to rationalize the underlying physics of this phenomenon and utilize it in particle manipulation applications. Based on these studies, it has been found that two opposing forces are exerted on a rigid, neutrally buoyant particle moving along a straight channel in a shear flow: (1) wall repulsion force, arising from the asymmetry of the corresponding wake vorticity distribution[56] which tends to push the particles away from the walls and (2) shear-gradient lift force originating from the curvature of velocity profile in confined flows which causes the particles to migrate away from the central axis.[45,50] The equilibrium position of the particles is determined by the balance of these forces and depends on the magnitude of Reynolds number as well as the blockage ratio, defined as $\kappa = a/D_h$, which describes the relative size of the particle to the channel, with a being the particle diameter. Fig. 1 schematically shows the geometrical dimensions of a spherical particle in a square channel.

Using matched asymptotic expansion method to capture both wall effects and Oseen-like inertial region, extensive analytical studies have been performed in the past decades to quantify the lateral migration of particles in the finite Reynolds number regime. The results indicate[50] a lift force scaling as $F_L \propto \rho U^2 a^4 / H^2$, assuming $\kappa \ll 1$ and $R_p \ll 1$, where $R_p = Re(a/D_h)^2$ denotes the particle Reynolds number, and it is a measure of flow disturbance induced by the particle motion. Thus, these constrained models are unable to address the finite size effects which later in the numerical work of Di Carlo et al.[58] has been shown to have significant impact on the particle dynamics. They investigated nonlinear effects in highly confined flows where the particle size approaches the channel dimensions and introduced new scalings for the lift forces. Based on their simulations, the force scaling varies with the lateral position of the particle. In the near-wall region, the lift force scales as

$$F_L = C_L \frac{\rho U^2 a^6}{H^4},\tag{1}$$

whereas close to the channel centerline

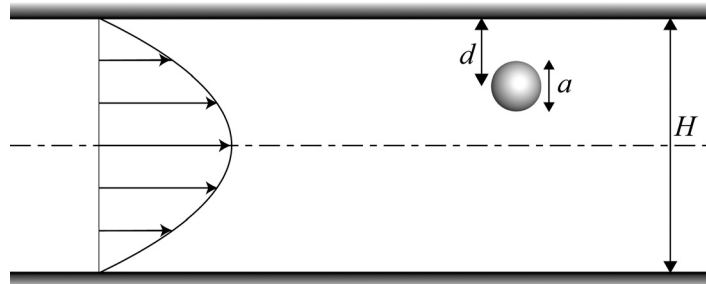$$F_L = C_L \frac{\rho U^2 a^3}{H}.\tag{2}$$

FIG. 1. Schematic illustration showing channel and particle dimensions and the fully developed velocity profile.

In above equations, C_L is the dimensionless lift coefficient which depends on the particle distance from the wall and the channel Reynolds number. The complex variation of C_L with Re is demonstrated to be in agreement with the experimental observations of Matas et al.[53] where it has been shown that as Re is increased, the equilibrium position of the particles moves toward the wall. The focusing behavior of the particles has been also studied for channels with square or rectangular shape,[57] illustrating 4-fold equilibrium positions distributed symmetrically across the channel cross section. Moreover, the channel aspect ratio has been identified[58] to play an important role in altering the location of particle attractors by weakening the shear-gradient induced lift force. Thus in channels with aspect ratio other than unity, the number of focusing positions is reduced to two locations distributed symmetrically along the longer dimension of the channel cross section. It has been shown numerically[59] that in high aspect-ratio channels, a blunted velocity profile is formed across the longer face, leading to suppression of the strength of shear gradient and amplification of wall-effect lift forces due to restricted particle rotation as well as diminished local velocity.

Examining Eqs. (1) and (2) reveals the strong dependence of inertial lift forces on the particle size, suggesting inertial migration as a continuous, passive mechanism for particle separation and cell purification applications in microfluidic devices. In this regard, high aspect-ratio channels are greatly beneficial as they lower the dispersion of particles and force them to focus along reduced number of equilibrium positions. Nonetheless, it is experimentally observed[60] that in the channels with an aspect ratio higher than a threshold, a bifurcation occurs where each focused stream breaks into two distinct bands, undermining the conditions for separation applications. The corresponding underlying mechanism for this phenomenon is not clear yet, and further study is required to shed light on this issue.

Despite the fact that traditionally inertia is neglected in the microfluidic systems, recent studies suggest a variety of applications that use the effects of fluid inertial forces. These applications including but not limited to cell and particle focusing,[61–63] sorting,[64] separation,[65–67] self-assembly,[68] filtration,[69–71] and enrichment and trapping[72] are poised to be high-throughput due to their operation under high flow rates. Recent progress and potential future directions in the area of inertial microfluidics are discussed in a recent review article by Di Carlo.[73] Even though prototype systems utilizing inertial microfluidics show more rapid and high-throughput outcomes compared to other promising techniques, such as microfiltration,[26,74,75] deterministic lateral displacement,[30,76–78] and hydrophoresis,[79,80] they lack the ability to increase the concentration of the target cells to a significant value. This issue is recently resolved by combining microscale laminar vortices with inertial focusing. Hur et al.[72] utilized microvortices generated by inertially driven flow at sharp corners to selectively isolate and trap larger target cells. Their system consists of a straight microchannel with rectangular cross-section sufficiently long to allow inertial effects to sort cells based on their size (Fig. 2(a)). Sorting is due to the migration of cells/particles to distinct lateral equilibrium positions resulting from a balance between two aforementioned counteracting lift forces.[63] The dimensions of the system are wisely designed such that the equilibrium positions are in the proximity of the channel walls. Downstream of the channel, trapping reservoirs are fabricated as rectangular cavities on the channel wall. As a result, vortices are created within these reservoirs as flow passes through them. When the particles reach the cell trapping reservoirs placed downstream of the channel, they are exposed only to a shear-gradient lift. Larger particles experience a larger lateral lift force which drives them across streamline towards the vortex center in the reservoir. Therefore, particles/cells with larger size are trapped within these microvortices, while smaller ones are flushed out through the channel. By operating this device in high flow rate regime ($Re \sim 200$) and utilizing parallel reservoirs and channels, a throughput of $\sim 10^8$ cells/min has been attained which, in microfluidic scales, is immense. Nonetheless the capturing efficiency, defined as the ratio of trapped cells to the injected ones, does not exceed 43% mostly due to high concentration and deformability effects which hinder the migration toward the walls and thereby cell trapping in the reservoirs. Similar studies have been conducted to focus[81] and separate[82] rigid spherical particles using finite Reynolds number flows in a series of alternating contraction-expansion channels. An example of multistream focusing using this design is shown in Fig. 2(b). The so-called multiorifice
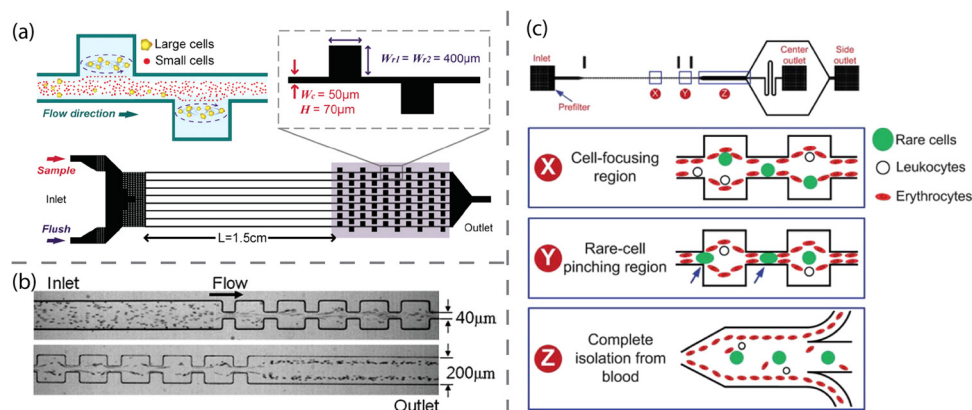
FIG. 2. Some examples of applications of inertial migration in microfluidics. (a) Schematics showing the dimensions and the working principle of a microdevice designed to separate and enrich larger cells by exploiting the difference in the inertial lift forces. Reprinted with permission from Hur *et al*., Biomicrofluidics **5**, 022206 (2011). Copyright 2011 American Institute of Physics. (b) Experimental images of the particles flowing through a multiorifice microchannel at $Re \sim 63$. Due to lateral migration induced by the contraction/expansion cavities, two separate focused streams of particles are formed at the outlet. Reprinted with permission from Park *et al*., Lab Chip **9**, 939–948 (2009). Copyright 2009 Royal Society of Chemistry. (c) Schematics illustrating the design and mechanism of a rare cell isolating microdevice. It consists of focusing, pinching, and extraction regions to trap the larger cells of interest in the vicinity of channel axis. Reprinted with permission from Bhagat *et al*., Lab Chip **11**, 1870–1878 (2011). Copyright 2011 Royal Society of Chemistry.

flow fractionation technique, although yielding relatively high throughput, requires operating in a certain narrow range of flow rates to exhibit decent performance in terms of focusing band width and separation efficiency. Bhagat and coworkers[60] improved this method by introducing a pinching region in addition to the focusing region to maintain the cells of interest around the channel centerline (Fig. 2(c)). They used this setup to separate and enrich extremely rare CTCs from a whole blood sample with throughput of $\sim 10^8$ cells/min and collection efficiency of $\sim 80\%$. In their design, by utilizing a high aspect-ratio contraction-expansion array, all blood cells are initially focused close to the channel sidewalls due to inertial lift forces, and then by adjusting the width of the pinching region to be on the order of the largest cell size, CTCs are refocused along the channel axis while the rest of the cells remain aligned around the sidewalls. Finally, by employing bifurcating outlets, CTCs, segregated from the red blood cells and peripheral blood leukocytes, can be extracted. The most important drawback associated with this method is the dependence of pinching zone dimension on the targeted cell size which necessitates fabrication of a new microdevice for every type of desired cell.

In addition to previous applications, inertia induced lift forces have been efficiently employed in solution exchange operations in order to transfer cells and particles across reacting solutions in a coflow.[59] This passive hydrodynamic method is advantageous in terms of exposure time to the shear flow which is extremely shorter compared to conventional cytometry methods involving external fields. Thus, the cell viability and the corresponding gene expressions are much less prone to damage due to transient experience of shear effects. However, the throughput of this technique is limited to high concentration threshold where particle-particle interactions become dominant over the favorable lift forces.

B. Viscoelastic focusing

Non-Newtonian effects provide another mechanism for the cross-stream particle migration in microfluidic confined channels, which has triggered several investigations in recent years. This phenomenon was first observed experimentally by Mason and coworkers[83–85] as they noticed different particle migration directions depending on the properties of the polymeric fluid. Based on their experiments in pressure-driven tube flow, the rigid spheres migrate laterally towards the wall in a highly shear-thinning liquid while are attracted towards the centerline in an elastic fluid with almost constant viscosity (Boger fluid). The latter case has been

scrutinized in detail in the experimental work of Tehrani[86] who found that in the suspensions of 5%-12% particle volume fraction, the migration occurs toward the region of lower shear rate. Thus in fluids with dominant viscoelastic characteristics, particles are pushed towards the centerline in case of Poiseuille flow while aggregate close to the outer cylinder wall in Couette flow.

The motion of a single particle and two particles in viscoelastic fluids has been studied analytically[87] and numerically.[88–90] To shed light on the underlying mechanisms of the transverse migration, Ho and Leal[87] studied the lift force exerted on a neutrally buoyant rigid sphere moving along a unidirectional two-dimensional confined flow using second-order fluid constitutive model and assuming small blockage ratio. Neglecting inertia effects, they employed a regular perturbation method in conjunction with the reciprocal theorem to evaluate the lateral force which was shown to be associated with the intrinsic normal stress differences. It is argued that the transverse motion stems from hoop thrust[87] arising from the gradient of shear rate across the sphere. This elucidation is confirmed by numerical work of Huang *et al.*[88] where it is shown that in the limit of negligible inertia and small blockage ratio, normal stresses induced by the curvature of the velocity profile force the particle to move towards the centerline where the shear rate is zero. On the other hand, as the width of the channel becomes smaller and the blockage ratio increases, the particle tends to move closer to the wall due to more intensified compressive normal stresses in regions of the channel away from the sidewalls. This type of attraction towards the wall for large values of κ has been observed in experimental study of Dhahir *et al.*[91] for $\kappa = 0.6$ whereas analytical studies have been unable to predict it due to limitations of the perturbation methods. Based on numerical simulations,[88,92] increasing the Weissenberg number (defined as the product of polymer relaxation time with the shear rate) will accelerate the particle motion towards the corresponding equilibrium position in both circumstances.

Here, we present a heuristic model to quantify the scale of the particle's lateral motion engendered by the first (N_1) and second (N_2) normal stress differences. For the sake of simplicity, we neglect the contribution of the second normal stress difference due to the point that for most polymeric fluids $|N_2|/N_1 < 0.1$.[93] The lift force exerted on a rigid small sphere because of elastic effects can be assumed to stem from the imbalance in the distribution of N_1 over the size of the particle,[86,94] $F_e \propto a^3 \nabla N_1$. In the limit of negligible inertia, the resulting velocity of lateral migration (v_L) can be derived by balancing this force with Stokes drag, $F_d = 6\pi\mu a v_L$, where μ is the fluid viscosity. Using upper convected Maxwell model to obtain the value of $N_1 = 2\mu\lambda_r\dot{\gamma}^2$ for steady Poiseuille flow[93] and assuming near constant viscosity, we can calculate the magnitude of the migration velocity as

$$v_L = \frac{c\lambda_r}{3\pi}a^2\nabla\dot{\gamma}^2,$$ (3)

with c being the proportionality constant, λ_r the relaxation time of the polymers, and $\dot{\gamma}$ the shear rate. Hence, particles with small blockage ratio in viscoelastic fluids transversely migrate towards the regions of small shear rate which correspond to central axis in tubes and both centerline and corners in case of rectangular channels.[95]

Besides the aforementioned factors, shear-thinning property of the fluid plays an important role in changing the equilibrium position of the suspended particles. It has been first observed in early experiments of Mason and coworkers[84] and later confirmed by further numerical and experimental studies[92] that neutrally buoyant rigid particles migrate towards the wall in Poiseuille flow of shear-thinning fluids. D'Avino *et al.* systematically studied this effect in a 2D domain[96] and in an axisymmetric tube[97] using Giesekus viscoelastic model which allows for the variation of viscosity with shear rate. Their results indicate a neutral cylindrical surface (at $r = r^*$) which acts as a separatrix to segregate the focus of the particles based on their initial conditions. The particles initially suspended at radial position $r > r^*$ are attracted towards the wall, while others migrate toward the axis line. It is found that by increasing the strength of shear thinning, the neutral position moves toward the central axis, promoting the aggregation of particles on the sidewalls. Bistability of these two equilibrium positions at intermediate shear-thinning regime has been verified in experimental observations of particle distribution in a 1%

water solution of PEO (polyethylene oxide)[97] (see Fig. 3(a)). In the corresponding flow regime with moderate strength of shear thinning, there exists an annular particle-free zone[92] because of coexistence of particle aggregates at both centerline and close to the walls. It is argued[88] that shear thinning leads to higher shear rate near solid boundaries which results in enhanced migration towards the wall due to modified distribution of compressive normal stresses especially on the side of the particles opposite to the wall.

In summary, the magnitude and direction of the lift force exerted on a rigid particle moving with viscoelastic fluid flow with negligible inertia depends on three dimensionless parameters: Weissenberg number, the blockage ratio, and a nondimensional parameter modulating the extent of shear thinning. Desired particle focusing scenarios can be achieved by fine-tuning these parameters in a microfluidic device.

Non-Newtonian effects, either exclusively or in conjunction with other hydrodynamic mechanisms, have been recently utilized in several studies for the sake of cell/particle focusing and separation. Using the viscoelastic properties of medium fluid and the corresponding elastic lift force, D'Avino and coworkers[97] could attain 3D focusing of particles flowing along a capillary tube. To enhance the particle migration toward the centerline, they adjusted rheological properties of the carrier liquid, geometrical characteristics of the experimental apparatus, and flow rate. Thus, small blockage ratio (∼4%), inertialess regime, and viscoelastic fluid with relatively low degree of shear thinning were preferred to perform the experiments. Utilizing these conditions ensures the particle migration towards the regions of minimum shear rate which in case of a circular tube correspond solely to the centerline. Although this mechanism is found to be effective over a relatively wide range of flow rates, its application is limited to low Reynolds number regime and thus cannot be considered a high-throughput method. In the same context, Kim et al.[98] used viscoelastic focusing technique to aggregate rigid colloidal nanoparticles at the centerline and corners of a square microchannel. The effectiveness of the focusing scheme was distinguished to be dependent on the particle size where for small particles no significant ordering in their distribution was observed. This can be attributed to pronounced effects of Brownian motion as well as weakening of elastic forces as the size of particles decreases.
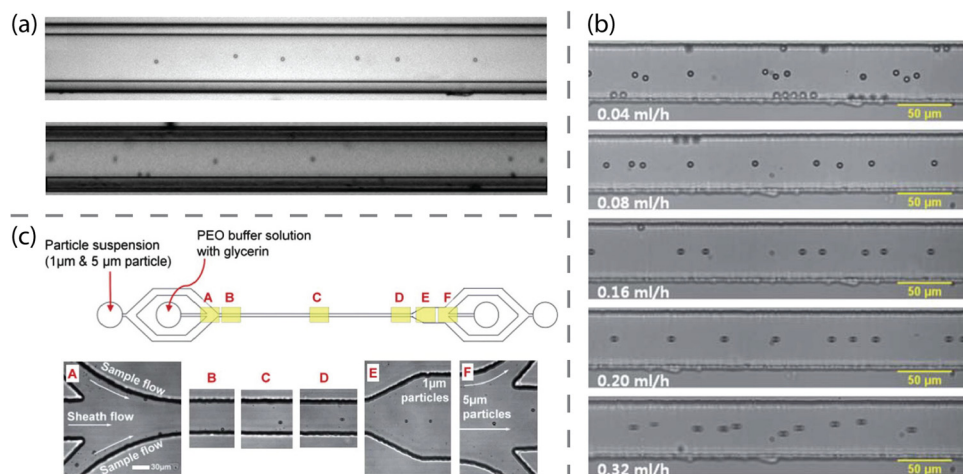

FIG. 3. (a) The top image illustrates the particle focusing along the centerline in a viscoelastic fluid with almost constant viscosity, while the bottom image shows the bistability of particle distribution in a shear-thinning fluid. The images are the results of experimental observations of particulate flows in a cylindrical microchannel. Reprinted with permission from G. D'Avino et al., Lab Chip **12**, 1638–1645 (2012). Copyright 2012 Royal Society of Chemistry. (b) Experimental images of the elasto-inertial particle focusing in a straight rectangular channel. By increasing the flow rate and hence the elasticity number, focusing along the centerline is achieved due to synergetic effects of the forces induced by inertia and viscoelasticity. Reprinted with permission from Yang et al., Lab Chip **11**, 266–273 (2011). Copyright 2011 Royal Society of Chemistry. (c) The top figure shows a schematic demonstrating the design of a microdevice used to separate cells and particles flowing in a viscoelastic fluid. The design includes sheath and sample flows. The particles are segregated based on their size due to difference in their lateral migration. Reprinted with permission from Nam et al., Lab Chip **12**, 1347–1354 (2012). Copyright 2012 Royal Society of Chemistry.

The insight resulting from this work can be employed in the design of nanoparticle separation devices.

In nanoscale territory, random Brownian effects can play a key role in scattering the colloidal particles and inhibiting their alignment. The relative importance of Brownian diffusive transport can be evaluated using Péclet number which indicates the ratio of diffusive to convective time scales as $Pe = \dot{\gamma}a^2/D$, where $D = k_B T/6\pi\mu a$ is the Brownian diffusivity coefficient with k_B being the Boltzmann constant and T the temperature. Diffusive effects gain significance because of Brownian motion of nanoparticles flowing in a microchannel (corresponding to $Pe \ll 1$) or due to shear-induced particle interactions in case of dense particulate flows. However, in the dilute regime, diffusion induced by Brownian motion becomes negligible when $a \gtrsim 1\,\mu\text{m}$.[94]

In the fabrication process of microdevices, it is more straight-forward to build microchannels with rectangular cross section which leads to multiplicity of equilibrium positions in particulate flows. To remedy this problem, researchers utilized the combination of elastic and inertia forces to enhance the localization of particles by directing their focus toward the channel centerline. The relative magnitude of elasticity to inertia forces can be quantified using elastic number defined as

$$El = \frac{Wi}{Re} = \frac{\lambda_r \mu}{\rho D_h^2}. \tag{4}$$

El is not a function of flow rate and only depends on the rheological properties of the polymeric solution and the geometry of the channel. The so-called elasto-inertial regime leading to 3D particle focusing occurs at a moderate range of El where effects of both mechanisms are important. Introducing inertia results in wall repulsion forces which prevent aggregation of particles around channel corners. Yang et al.[99] embraced this idea to design a sheathless particle focusing microfluidic device operating in the range of $El \approx O(1-10)$. By tuning the extent of polymer solution and the flow rate, they achieved 3D focusing of 95% of particles along the centerline of a straight microchannel (Fig. 3(b)). Further, by exploiting the physics of the lift forces being strongly dependent on the size of the particles, they managed to separate the small and large microbeads with separation efficiency of 83% (defined as the ratio of number of particles at the outlet to the total number of the particles of the same size injected at the inlet). In a more recent work,[100] higher purities for particle sorting were obtained (up to 99.9%) by employing the same elasto-inertial effect in a more complex setup consisting of sheath and sample flows passing through a microchannel with separate exits to collect larger particles around centerline and smaller ones close to the sidewalls (see Fig. 3(c)). These studies seem promising, although further research is required to broaden their scope of application, for example to wider range of flow rates and to more general types of polymeric fluids with less restrictions on the respective rheological characteristics.

C. Deformability-selective cell separation

The cell deformability is an important biomarker and monitoring its alterations can be of great benefit in diagnosing some lethal diseases such as malaria,[101] diabetes,[102] and cancer.[103] Specifically, cancer cells have been shown[104] to be much more deformable comparing to the normal cells of the same tissue. In addition, stiffness of red blood cells (RBCs) is found to be largely affected by blood diseases such as anaemia.[105] As it will be described, harnessing hydrodynamic mechanism based on deformability-induced lateral migration provides us non-invasive methods to separate infected cells from the healthy ones.

Deformability of a particle moving along a confined flow introduces another nonlinearity causing cross-stream migration even in the limit of Stokes flow. This phenomenon was first demonstrated theoretically for droplets,[40,106] and later was numerically and experimentally observed for bubbles, vesicles, and viscous capsules.[107–113] The essential factor responsible for the deformation and consequent lateral migration of droplets is found to be stress matching

type of boundary conditions at the corresponding interface instead of no-slip condition at the boundary of a rigid wall.[109] Various studies[40,114,115] assert the point that the direction of migration depends on the type of deformable particle and its relative viscosity with respect to the surrounding fluid. The latter parameter can be quantified by the ratio of internal to external viscosities, $\lambda = \mu_{in}/\mu_{out}$, where μ_{in} refers to the viscosity of droplet fluid or fluid inside an elastic membrane in the case of vesicles and RBCs. Moreover, to account for the degree of deformation, different geometrical measures have been proposed, such as (i) reduced volume[116,117] defined as the ratio of actual particle volume to that of a sphere with the same surface area

$$\nu = \frac{V}{\frac{4}{3}\pi\left(\frac{S}{4\pi}\right)^{3/2}} \tag{5}$$

and (ii) excess area[118,119] which denotes the area difference of the particle and a sphere with equivalent volume,

$$\Delta = \frac{S}{R^2} - 4\pi, \qquad R = \left(\frac{3V}{4\pi}\right)^{1/3}. \tag{6}$$

In aforementioned equations, R is the effective particle radius and V and S are deformed particle volume and area, respectively. For red blood cells, $\nu \approx 0.7$ (Ref. [95]) and $\Delta \approx 5$ (Ref. [120]).

   The study of deformability as a migration mechanism was first initiated in the context of drops. It is illustrated, both experimentally and theoretically, that droplets with viscosity ratio $\lambda > 5$ exposed to confined flows shift towards the channel centerline.[66,106,121] The degree of deformation and the final equilibrium position of the drops are found to be strongly dependent on the viscosity ratio where more viscous drops undergo less shape deformation and travel shorter distances laterally.[114,121] However, the steady state of even highly viscous drops is much closer to the centerline compared to the final position of rigid particles, mainly due to the presence of slip velocity at the interface of dispersed and continuous phases.[66] It is conjectured that existence of non-solid boundaries largely contributes to the lateral drift force.[66] Contrary to our intuition, for drops with viscosity ratio smaller than a certain threshold ($\lambda < 5$), experimental[66] and numerical[111] studies have indicated a reversal in the direction of migration which in this case is towards the channel wall. This shift in lateral motion occurs in spite of shape deformation analogous to higher viscosity drops. It is argued[111] that this switch of equilibrium position occurs due to the point that lubrication forces acting in the gap between drop and the wall become inconsequential for less viscous droplets and therefore cannot push them away from the wall.

   Another type of soft particles where their lateral motion is of great interest are biological capsules with membranes composed primarily of lipid bilayers, also known as vesicles.[122] They are generally used in biophysical studies of membranes and red blood cells dynamics.[123] Suspended in steady shear flow, vesicles have been observed to exhibit different dynamical modes including tank-treading motion where the vesicle deforms into an ellipsoidal particle with a stationary orientation with respect to the flow direction while its membrane is circulating about its interior.[124] It is notable that in case of a rigid ellipsoid, the particle does not maintain a fixed inclination but will start to tumble in an unsteady fashion.[125] Thus, deformability plays an essential role in ensuing the tank-treading motion.

   Experimental observations[112,116,117] have indicated that vesicles undergoing tank-treading motion in a shear flow adjacent to a wall experience a lateral repulsion force which pushes them away from that wall. Based on theoretical studies, this force stems from the flow disturbances engendered by asymmetric deformation of the vesicles.[40] Different expressions have been proposed to quantify the magnitude of the resulting transverse drift velocity. However, they all can be described in terms of separation distance from the wall d, effective radius R, and the shear rate $\dot{\gamma}$. In the case of a vesicle close to the wall ($d \sim R$)[116,117]

$$v_L = C_L \frac{R^2 \dot{\gamma}}{d}, \tag{7}$$

and if it is far from the wall $(d \gg R)$[119,125]

$$v_L = C_L \frac{R^3 \dot{\gamma}}{d^2}. \tag{8}$$

Here, C_L denotes the dimensionless lift coefficient which has been formulated in various formats, for instance in terms of reduced volume ν,[116] as a function of viscosity ratio λ and ellipsoid geometrical measures,[125] or in terms of excess area Δ and λ.[119] Assuming flow with negligible inertia, the corresponding lift force can be calculated using Stokes law as $F_L = 6\pi\mu R v_L$. In these models, it is presumed that the lift force always acts in the opposite direction of the wall to push the particle towards the centerline. Indeed, analytical[126] and numerical[127] studies have shown that vesicles, unlike surfactant-free drops, always migrate towards the central axis in Poiseuille flow, regardless of the value of the viscosity ratio.

Exploiting deformability-induced particle migration opens new ways to focus and separate cells based on their inherent structural characteristics which results in passive, label-free cell sorting processes in microfluidics. In most of the pertinent studies, this hydrodynamic mechanism is used in conjunction with other effects, such as viscoelasticity and inertia. But there are few works where cell separation microdevices are solely designed based on the deformability-induced cross migration. For example, Geislinger et al.[128] separated RBCs from other blood components by harnessing deformability-selective cell-wall interaction in a non-inertial flow inside a microchannel (Fig. 4(a)). The repulsion force exerted on RBCs in the mode of tank-treading motion is much larger compared to platelets, causing RBCs to be focused closer to the centerline. This technique has been shown to be robust over a relatively wide range of flow
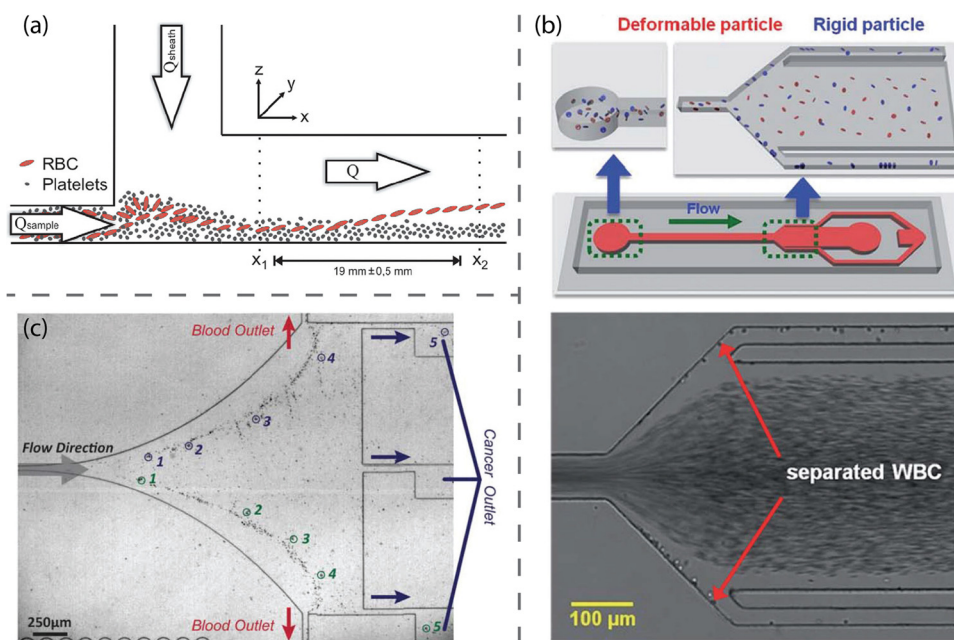

FIG. 4. Some applications of the deformability-induced migration in the microfluidics. (a) Schematics showing the dimensions and mechanism of operation of a microdevice designed to separate RBCs from the platelets. Reprinted with permission from Geislinger et al., Appl. Phys. Lett. **100**, 183701 (2012). Copyright 2012 American Institute of Physics. (b) The top figure shows a schematic illustrating the mechanism of deformability-selective cell separation in a viscoelastic medium. The bottom figure is an experimental snapshot demonstrating the separation of WBCs from RBCs due to difference in their deformability characteristics. Reprinted with permission from Yang et al., Soft Matter **8**, 5011–5019 (2012). Copyright 2012 Royal Society of Chemistry. (c) Deformability-selective separation of blood and cancer cells in an inertial flow. Reprinted with permission from Hur et al., Lab Chip **11**, 912–920 (2011). Copyright 2011 Royal Society of Chemistry.

rates as far as the corresponding Reynolds number remains small. Working in the same inertia-less regime, Yang et al.[95] employed lateral lift forces arising from the combinational effects of deformability and viscoelasticity to focus RBCs at the center of a microchannel in order to separate them from white blood cells (WBCs). As mentioned before, the particles flowing in a viscoelastic medium inside a rectangular channel migrate toward the centerline as well as the corners. Introducing deformability results in additional wall repulsion forces which selectively entrains the particles at the corners. Considering the point that the deformability-induced lift force depends on the asymmetry of the particle, it can be inferred that this force is negligible for WBCs due to their near spherical shape. Hence, while RBCs mainly concentrate at the core of the channel, WBCs can be selectively extracted along the corners. Using this setup, Yang and coworkers[95] could obtain WBCs with a purity of 35% from a dilute input solution with WBC/RBC ratio of 0.17%. The design of their device and a snapshot of separated cells are shown in Fig. 4(b). Although promising, this technique needs further development and improvement to be comparable with commercial enrichment methods.

Incorporating the effect of inertia into the previous cell separation techniques can substantially enhance the throughput. Utilizing this idea, Hur et al.[66] designed a microfluidic device for classification and enrichment of different types of cells based on their size and deformability. Taking advantage of high aspect ratio channels leading to lower number of equilibrium positions, they calibrated the device based on the unique lateral location of each category of cells in order to detect and separate them using different outlets across the width of the channel. By tuning Reynolds number to an optimum value, they achieved throughput of $\sim$22 000 cells/min while yielding 96% recovery rate for the separation of metastatic breast cancer cells (see Fig. 4(c)). This technique appears to be more effective for more deformable cells compared to stiffer cells in terms of enrichment performance. Also, in this method the range of flow rates should be carefully scrutinized in order not to alter the gene expression of the cells under the effect of shear flow.

D. Dean flow

In inertial flows inside the channels with curved geometry, centrifugal forces create a secondary rotational flow, called Dean flow,[129,130] which is of paramount importance in the flow focusing applications in microfluidics. In curved rectangular channels, a parcel of fluid passing through the central region of the channel is pushed outward due to centrifugal effects, and thus, to satisfy the incompressibility condition, the fluid in the near-wall region is driven inwards. Hence, two symmetric vortices on the top and bottom halves of the channel's cross section are established, leading to the formation of a pressure gradient in the radial direction. The strength of this secondary flow can be quantified by the Dean number[130]

$$De = Re \sqrt{\frac{D_h}{2R_c}}, \tag{9}$$

where R_c denotes the radius of curvature of the channel. De can be physically interpreted as the square root of the ratios of centrifugal and inertia forces to the viscous force. Its direct dependence on the Reynolds number implies that the effect of Dean flow becomes significant in the inertial regime where $Re \gtrsim O(1)$. The other important dimensionless parameter, where its value largely influences the shape of the vortices, is the curvature ratio, $\delta = D_h/2R_c$.[130] Different relationships between the velocity of Dean flow and the corresponding Dean number have been put forward. For example, Ookawara et al.[131] proposed the following correlation based on the numerical simulations of the problem with a specific configuration

$$U_D = 1.8 \times 10^{-4} De^{1.63}. \tag{10}$$

But simple scaling arguments[132] as well as experimental results of Gossett and Di Carlo[133] suggest that

$$U_D \sim De^2 \mu / \rho D_h. \tag{11}$$

This secondary flow exerts an additional drag force in the lateral direction on the particles moving along the channel axis. Using the latter expression for U_D, the drag attributed to Dean flow is found to scale as $F_D \sim \rho U^2 a D_h^2 / R_c$. This force always acts in a way that constraints the particles to follow the vortex path.

Inertial lift forces (F_L) are also present in the cross-stream directions, and their balance with Dean drag force determines the modified preferred locations of the particles. In fact, in channels with curved geometry, the number of equilibrium positions are reduced compared to straight channels because of destabilizing effect of the Dean force. Specifically, equilibrium positions along the midline of the channel between two counter-rotating vortices will disappear, leaving only two preferred locations for the particle focusing. This characteristic of the curved channels makes them more suited for applications in ordering and separation.

To quantify the interplay between the lift and Dean drag forces, Di Carlo and co-workers[73,133] introduced an inertial force ratio, defined as

$$R_f \sim \frac{F_L}{F_D} = \frac{2R_c a^2}{D_h^3}, \tag{12}$$

which characterizes different regimes of particulate flows in curved channels. It is noteworthy that in the derivation of this ratio, the effects of some other components such as channel's Reynolds number and the lateral position of the particle for the sake of simplicity have been ignored. It is argued[133] that weak dependence of R_f on these factors does not alter its prowess as a characterizing parameter of the system. Depending on the range of R_f, three regimes are distinguishable: (a) if $R_f \gg 1$, the secondary flow becomes inconsequential compared to inertial effects, (b) if $R_f \ll 1$, particles remain unfocused due to dominant strength of rotational flow, and (c) if $R_f \sim 1$, an intermediate regime occurs where the number of inertial equilibrium positions are reduced due to Dean drag forces. Gossett and Di Carlo[133] conducted numerous experiments using 2.2 μm particles to obtain a phase diagram of the flow for different values of R_f, and based on their conclusion, the intermediate range for their specific configuration starts at $R_f \gtrsim 0.037$. However, the universality of this result is questionable considering lack of generality in the corresponding experiments in terms of variation in particle's size and channel's aspect ratio.

Beside reducing the number of equilibrium positions, including curvature introduces another important advantage over straight channels that can be crucial in terms of energy efficiency. It is experimentally observed[133] that when De is large enough, particles flowing in curved microchannels reach their final stable positions while traveling shorter distances compared to straight channels with an equivalent flow rate. Consequently, flow focusing applications using curving geometries encounter lower pressure drop due to the skin friction and thus require less pumping power to drive the flow. Hence using this technique, higher throughputs can be attained while maintaining the pressure lower than the leakage threshold.

Dean flow effects have been recently utilized in microfluidic devices for cell/particle separation and focusing applications. In this regard, different curving profiles have been employed such as single curves,[134] spirals,[67,135–139] and serpentine curves.[61,63,133,140] Among these, spirals are the most widely used geometry in microdevices as they yield a sufficiently large channel length while occupying minimum surface area. The only disadvantage associated with spirals is their intrinsic difficulty with parallelization to fulfill high-throughput systems. However, this problem can be overcome to some extent by taking advantage of higher flow rates which are essential to utilize the full capabilities of Dean flow effects.

Papautsky and coworkers[67,135] were among the first research groups to employ spiral microchannels for the purpose of passive focusing and separation. They experimentally and numerically demonstrated[135] that the secondary flow can be used to separate two different particle sizes flowing in an inertial regime inside a 5-loop spiral channel with two inlets and two outlets. Based on their study, it was shown that large particles with blockage ratio of $\kappa > 0.07$

aggregate on the inner channel wall due to combined effects of lift and Dean drag forces, while smaller particles are more dispersed in the outer regions of the channel. Later, they improved their design[67] in terms of throughput as well as the number of separated particle streams (see Fig. 5(a)). Utilizing higher flow rates ($De \sim 4 - 20$) and employing an additional wider straight channel before the multiple outlets, they separated a mixture of three different particle sizes with a separation efficiency of $\sim$90%. In both works, low aspect ratio channels were preferred ($H/W = 0.5$ in Ref. 135 and $0.18 < H/W < 0.28$ in Ref. 67) to minimize the multiplicity of equilibrium positions. Due to quadratic dependence of R_f on the particle diameter, larger particles are driven further towards the inner wall by the inertial forces, whereas in case of smaller particles the dominant effect of Dean drag forces focus them closer to the centerline and the outer wall. This passive mechanism provides a robust basis for multistream separation and extraction of particles based on their size. The same setup has been also used[67] for the sorting of two types of neural cells, achieving separation efficiency of >80% with an incredible throughput of $\sim 10^6$ cells/min. The slight decrease of the separation efficiency can be attributed
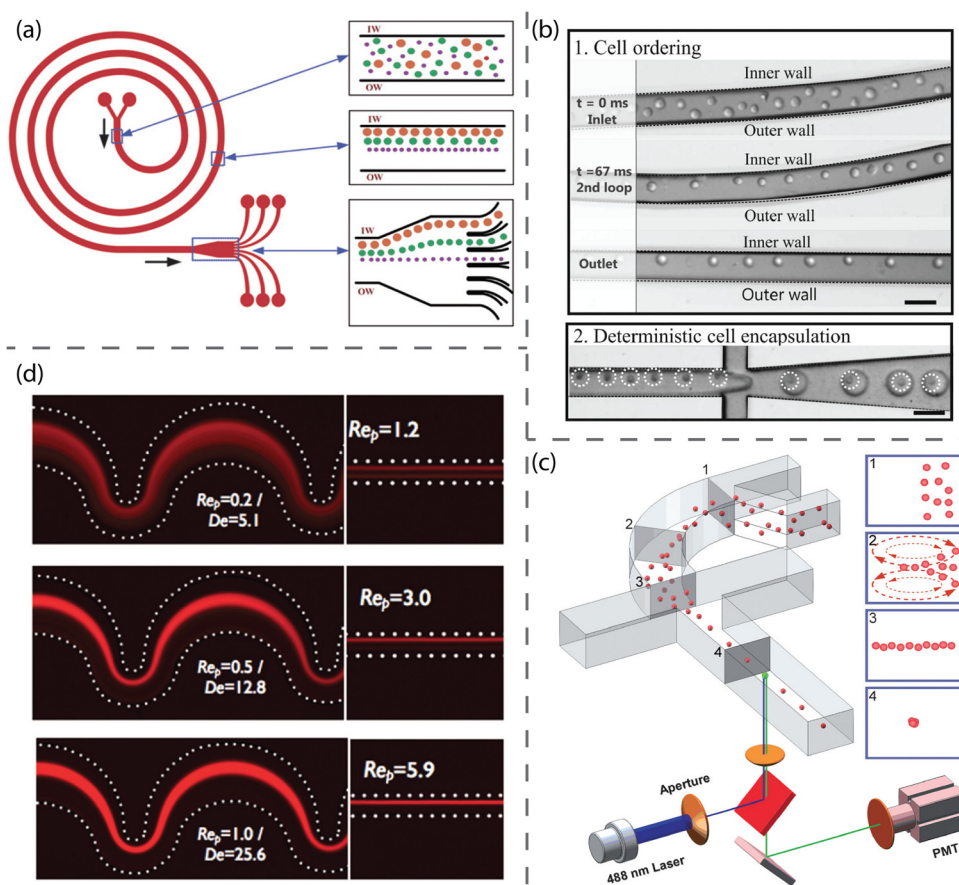

FIG. 5. Some applications of Dean flow in microfluidic systems. (a) Schematic of a microdevice to separate different particles based on their size using combined inertial and secondary flow effects. In this spiral microchannel, larger particles equilibrate along the inner wall, while smaller ones aggregate around the centerline. Reprinted with permission from Kuntaegowdanahalli *et al.*, Lab Chip **9**, 2973–2980 (2009). Copyright 2009 Royal Society of Chemistry. (b) Experimental pictures showing the cell ordering and encapsulation using a spiral microchannel. Reprinted with permission from Kemna *et al.*, Lab Chip **12**, 2881–2887 (2012). Copyright 2012 Royal Society of Chemistry. (c) Schematic of a microfluidic system to focus the particles using a curved microchannel as well as horizontal and vertical sheath flows. The lateral position of the particles at different locations are depicted in panels 1-4. Reprinted with permission from Mao *et al.*, Lab Chip **9**, 1583–1589 (2009). Copyright 2009 Royal Society of Chemistry. (d) Fluorescent images of the particulate flow in a serpentine microchannel show that by increasing flow rate and thus Dean number, particle focusing along a single stream is achieved. Reprinted with permission from Oakey *et al.*, Anal. Chem. **82**, 3862–3867 (2010). Copyright 2010 American Chemical Society.

to the cell deformability effects which prevent the aggregation of the cells close to the walls. The operational throughput of such systems working in the inertial regime is limited by two important factors: cell viability which might be damaged due to high shear rate effects, and clogging problems which are likely to arise in microfluidic designs with multiple constrictions at the outlet. Despite associated deficiencies, spirally shaped microchannels have been widely used in various microfluidic applications, such as sheathless flow cytometry,[136] cell cycle synchronization and fractionation of asynchronous mammalian cell lines,[141] delivery of exogenous DNA payloads into cells,[137] and single cell droplet encapsulation[139] (Fig. 5(b)).

The vortical flow resulting from Dean effects have been also used to focus particles passing though microchannels with a single curve.[134] Adjusting the size of the particles and the channel dimensions to maintain the value of $R_f < 0.01$ and employing two sets of sheath flows, Mao et al.[134] attained three-dimensional hydrodynamic focusing to ensure single cell passage through the laser beam of flow cytometers. The mechanism of their device is schematically shown in Fig. 5(c). In this drifting technique, 2D focusing is initially achieved because in the small R_f regime inertial lift forces are negligible, leading to particles entrainment by Dean vortices and their aggregation along the channel's midline. In the next step, horizontal sheath flows, injected normal to the axial direction, create 3D focusing along the centerline. Using the aforementioned setup, a throughput of $\sim 10^5$ particles/min for flow cytometry applications has been fulfilled. However, further study is required to confirm the robustness of this method when dealing with deformable cells instead of rigid particles.

Serpentine channels with variable radii of curvature and alternating curving directions provide high-throughput hydrodynamic focusing and separation techniques via parallelization on a single substrate. The pioneering work of Di Carlo et al.[63] illustrated the potential of this type of geometry for cell/particle ordering purposes in the inertial flow. It is observed[61,63] that in asymmetric curving geometries, the destabilization of the equilibrium positions due to Dean flow is amplified, leading to formation of a single stream of particles in shorter travelled distances compared to the straight or symmetrically curved channels (see Fig. 5(d)). As the threshold pressure associated with the leakage is the main limiting design factor in such systems, the serpentine geometry renders higher capacity to increase the throughput due to its inherently lower pressure drop. Using this technique, Di Carlo et al.[63] focused cells at a rate of $\sim 10^6$ cells/min with negligible damage to their viability. This method, although advantageous in terms of not requiring additional sheath flows, is operationally limited to a specific range of flow rates for optimum focusing performance. The corresponding interval of optimal channel Reynolds number can be approximately inferred from the phase diagram of particle ordering in curved microchannels[133] in terms of associated value of R_f and the degree of focusing.

III. VORTICITY INDUCED TRAPPING

Vortex-induced trapping provides promising approaches for high-throughput size-selective separation of cells and particles. These vortices can be generated using the geometrical modification of the channel profile,[72,142] by acoustic streaming[143] or via electrokinetic methods, such as induced-charge electro-osmosis,[144] AC electro-osmosis,[145] and dielectrophoresis.[146,147] The optimum conditions for particle trapping in confined microvortex flows have been analyzed analytically and numerically by Liu et al.[148] using the concepts of nonlinear dynamics. It has been shown that introducing non-hydrodynamic forces can substantially improve the efficiency of vortical, point, and ring traps. In this section, a brief review of studies regarding the production of vortices by means of streaming bubbles or solid boundaries is presented.

A. Cavitation microstreaming

Oscillating bubbles have shown a great deal of promise in fluid and particle/cell manipulation in microfluidic systems. They are greatly beneficial in a number of proposed applications in chemical, biological, and physical processes such as mixing,[149–151] pumping,[152,153] characterizing enzymatic reactions,[154] cell lysis,[155] and sorting and enrichment.[156,157] A thorough review article on applications of oscillating microbubbles in microfluidics is recently written by

Hashmi et al.[158] Although, there are a number of techniques to generate bubbles in microfluidic channels,[159,160] using a cavity is found to be the simplest. Upon generation of the bubble, a piezoelectric transducer can be coupled with the device to oscillate the bubble. Despite being simple, this manner of inducing bubble oscillation is rather accurate and efficient. Upon oscillation, a bubble can vibrate under linear or non-linear response depending upon the amplitude of the vibration.[161] The fast vibration of the bubble's interface produces a second order streaming flow that has a steady component. However, time-averaging leaves only the steady part since sampling rate is at rates much slower than oscillation frequency. The steady flow, known as "cavitation microstreaming,"[162,163] has streaming Reynolds number defined as $Re_s \equiv 2\pi\epsilon^2 a^2 f/\nu$, where ν, a, ϵa, and f are the kinematic viscosity of the liquid, bubble radius, oscillation amplitude, and frequency, respectively. Depending on f, bubble oscillates in different oscillation modes; however, oscillation amplitude and the corresponding cavitation microstreaming are more pronounced when the bubble is excited at its resonance frequency.[158,164] For $Re_s \ll 1$, flow is described as Rayleigh-Nyborg-Westervelt (RNW) streaming and can be modeled using the method of images and singularity.[165] The maximum streaming velocity, which is located near the bubble, can then be approximated from $u_s \sim 2\pi\epsilon^2 af$.[155] However, in high applied voltages and typical applied frequencies in microfluidic systems[156,157] (15 kHz $< f <$ 100 kHz), $Re_s \sim 1$ which makes the theoretical solution more complicated as the full Navier-Stokes equations must be solved. Nevertheless, RNW streaming can describe the flow in these cases quite accurately.[157] Within a typical microfluidic experimental setup[149,156] the streaming velocity is on the order of mm/s to cm/s, which makes the manipulation of the liquid and particles in microchannels using oscillating bubbles a powerful yet efficient and simple technique compared to electrokinetics and electrophoresis.[144,166–168]

Recently, Wang et al.[156,157] used the cavitation microstreaming of a bubble together with Poiseuille flow to manipulate particles and their spatial concentration for enrichment, filtering and focusing applications in microfluidic devices. The working mechanism is based on the fact that particles behave differently around the oscillating bubbles depending on their finite-size. When the relative streaming strength ratio, defined as $s \equiv \bar{u}_p/u_s$, where $\bar{u}_p$ is the mean Poiseuille velocity, is low, the streaming flow dominates near the bubble with two vortices. Under this condition, near the oscillating bubble, particles larger than a critical size ($a_p > d_{gap}$, where a_p is the particle radius and d_{gap} is a characteristic size of the gap, dictating the critical size) are forced to move across the streamlines towards the vortex of microstreaming and eventually be trapped in the streaming. This is due to the fact that the particles cannot penetrate the bubble, so they move across streamlines because of finite size effects. The gap width d_{gap}, which is the distance between the surface of the bubble and closed streamlines in the vortex, can be theoretically predicted using a geometry argument[156] as $d_{gap} = sh[3(h/H) - 2(h/H)^2]$. Here, H is the width of the channel and h is the portion of the channel width in which the streamlines are rectified to pass through d_{gap} when the streaming is present near the bubble. The equation for obtaining d_{gap} is derived using the conservation of mass which dictates that the mass flux in portion h of the channel must pass through the gap between the closed streamlines and the bubble. This mechanism, described schematically in Fig. 6, can lead to high
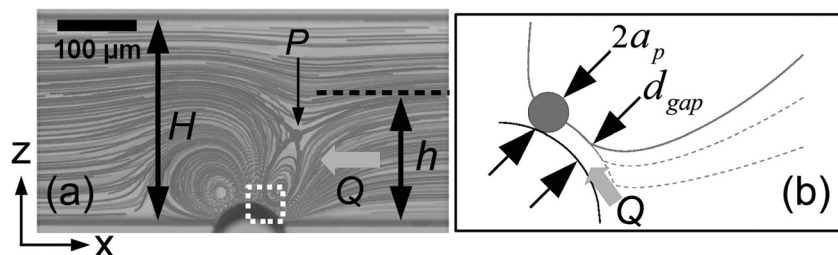

FIG. 6. Mechanism of trapping: (a) streak image highlighting the hyperbolic point P and critical streamline and (b) schematic detail of the boxed region of panel (a). Reprinted with permission from Wang et al., Appl. Phys. Lett. **99**, 034101 (2011). Copyright 2011 American Institute of Physics.
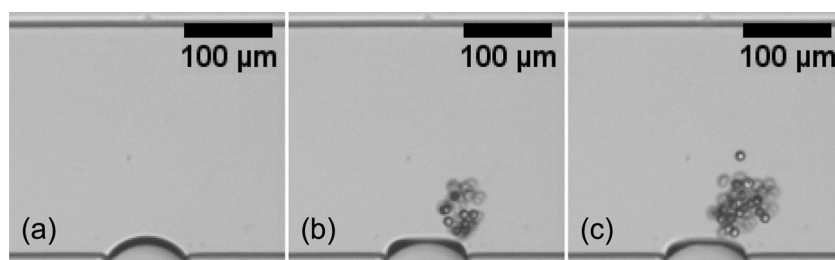
FIG. 7. Accumulation of microparticles around an oscillating bubble. Snapshots (b) and (c) are taken 2 s and 4 s after (a), respectively. Reprinted with permission from Wang *et al.*, Biomicrofluidics **6**, 012801 (2012). Copyright 2012 American Institute of Physics.

concentration of the target particles in vicinity of the bubbles which can be used for particle enrichment (Fig. 7). However, as the number of trapped particles increases, particle-particle interactions eventually lead to the release of particles from the vortex. These interactions, such as collisions and hydrodynamic interactions, cause perturbations in the particle trajectories which allow particles to enter the region of open streamlines. The release of the particles occurs at a narrow region near the bubble pole where the perturbations are stronger. Wang *et al.*[157] used the releasing technique for focusing applications since the release trajectory is narrower than the trajectories far upstream of the bubble.[157] Depending on d_{gap}, more than one size of particles can be trapped within the vortical flow. As these particles are transported in the streaming flow, they gradually settle into different closed trajectories depending on their size as illustrated in Fig. 8. The small particle orbits on a larger loop while the large particle orbits on a smaller trajectory.

The same cavitation microstreaming approach based on finite size effects can be used to collect motile bacterial cells in the vortical flow of an oscillating bubble as shown by Yazdi and Ardekani.[169] In this case, they observed rapid formation of biofilm streamers which occurs due to the presence of the microstreaming vortices. They also showed that bacterial motility affects the rate of collection of bacteria in the vortices suggesting that bacteria with high motility are trapped faster and more intense in the vortical flow. Fig. 9 shows the collection of bacteria in the microstreaming of an oscillating bubble and the biofilm streamer formed after three minutes.
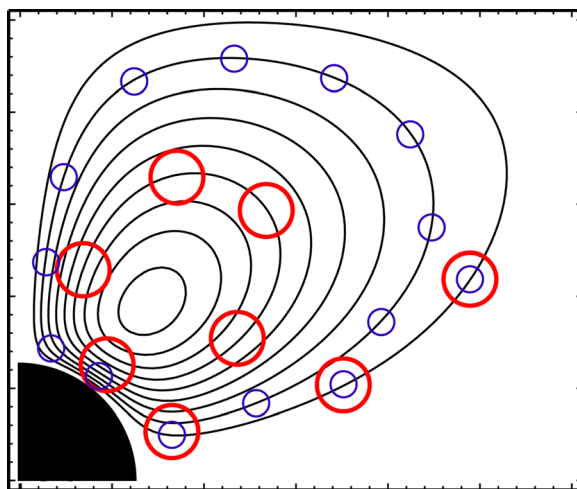

FIG. 8. Schematic illustration of characteristic loops of large and small particles. Reprinted with permission from Wang *et al.*, Biomicrofluidics **6**, 012801 (2012). Copyright 2012 American Institute of Physics.
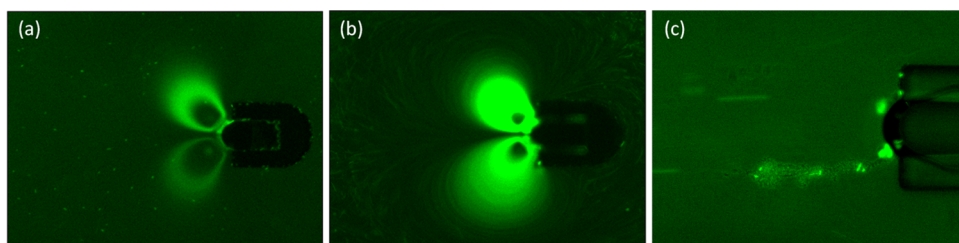
FIG. 9. Bacterial collection in a vortical flow of an oscillating bubble trapped in a horse-shoe structure for (a) low motile bacteria (*E. coli* DH5α) and (b) high motile (*E. coli* RP437). (c) Rapid biofilm formation in the vicinity of the bubble. Reprinted with permission from S. H. Yazdi and A. M. Ardekani, Biomicrofluidics **6**, 044114 (2012). Copyright 2012 American Institute of Physics.

B. Hydrodynamic tweezers

An alternative way of trapping cells by acoustic streaming is by utilizing an oscillating solid boundary in a microfluidic system. The solid boundary can be a fixed cylinder in the middle of the channel (see Fig. 10(a)) or a sharp edge of a cavity in the channel wall. By applying low audible frequencies (250 Hz $\leq f \leq$ 1000 Hz), time-averaged secondary streaming, known as "steady streaming," similar to cavitation microstreaming, is generated adjacent to the solid boundary. These streamings are driven by Reynolds stresses that are created within the Stokes layer near solid boundaries. Representative streamlines of the streaming flow at different planes of symmetry have been shown in Figs. 10(b) and 10(c). Stokes layer thickness, $\delta_{AC} = (\nu/f)^{1/2}$, is a scaling parameter for oscillating flows that describes how far from a surface the viscous damping of an oscillating boundary persists.[170] Here, ν and f are fluid kinematic viscosity and cylinder's oscillation frequency, respectively.

Lutz *et al.*[171] used this technique for dynamic single-cell measurements. The secondary flow in the vicinity of a fixed oscillating cylindrical obstacle in a microfluidic channel, with radius of 125 μm, was used to trap and suspend single-cells, including motile cells. Upon applying the audible-frequency fluid oscillation, the trapping force draws the cell toward the cylinder. The magnitude of the trapping force, which is directly related to the amplitude of oscillation, is up to 30 pN, and it is of the same order of magnitude as forces induced by optical tweezers and dielectrophoretic traps. However, unlike these techniques, the magnitude of shear stress generated by the oscillating fluid is $\leq$1.5 N/m^2, which is within the physiological range for cells and arterial blood flow. Location of the trapping is near the eddy center, and it is controlled via the oscillation frequency. They have further shown that by adjusting the applied frequency, device geometry, and fluid kinematic viscosity, the depth of the trapping eddy can be matched to the diameter of the cell. Therefore, despite the different initial positions of the cells, they are ultimately positioned at a specific location within the channel's midplane. It should be
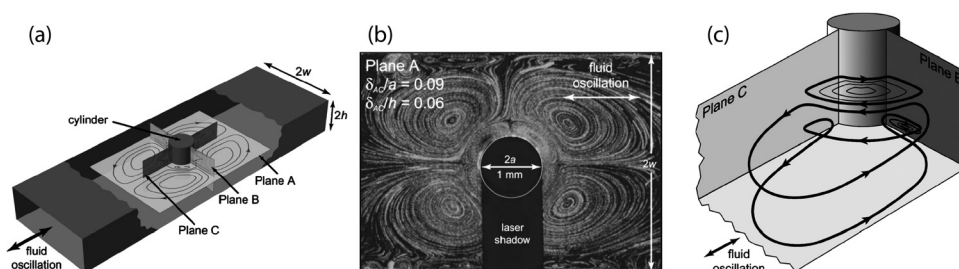

FIG. 10. (a) Schematic representation of the flow channel and the symmetry planes as observed in experiments. (b) The image of particle pathlines at plane A for particle size $a_p = 500$ μm. (c) Schematic streamlines of streaming flow at planes B and C. Reprinted with permission from Lutz *et al.*, Fluids **17**, 023601 (2005). Copyright 2012 American Institute of Physics.

noted that due to the low range of applied frequency and intensity, the acoustical effects associated with radiation force and bulk energy absorption are not important here. Recently, they expanded their design to cavities as well as other obstacles in a microfluidic channel and investigated the effect of design geometry on steady streaming flow shape, structure, and strength by conducting the experiments in channels with different oscillating boundaries.[172] In this work, they improved upon their previous observation and showed that the trapping location is closer to the solid boundary than the core of the eddy. The overall reported results of the particle trapping are quite similar among different posts; however, steady flow structure, strength, and trapping stability in cavities are significantly different.[172]

IV. PERSPECTIVES

Employing hydrodynamic effects in microfluidic applications has been distinguished in the past decade to be fruitful both in terms of throughput and efficiency and continues to thrive in the future through further improvements in separation resolution and processing rate. However, there are new areas for applications of hydrodynamic microfluidic phenomena which appear promising and demand further investigations, both theoretically to inform researchers of the underlying physics and experimentally to exploit them in biological applications. Although several active separation techniques have been developed to meet the growing demand in these new territories, they lack the associated advantages of the passive methods reviewed in previous sections, such as ease of design and maintaining the viability of genes. Sorting micro/nano-scale chiral objects by means of lateral drift induced by shear flow is among those areas requiring further studies. Chirality is a common property of many biomolecules, including well-celebrated DNA strands.[173] Separating these molecules based on their chirality is strongly useful in a variety of applications ranging from food industries to pharmaceutical products. Considering the inherent difficulties of the currently available methods, several attempts have been made to harness chirality-induced lift forces arising in a shear flow to separate the molecules.[174–176] Recently, Marcos *et al.*[176] presented a technique to fulfill this purpose, achieving an ample efficiency ($>80\%$) for the separation of microscale, dormant helical bacteria. Nevertheless, further work is required to expand the scope of this method in terms of operating at higher throughput and separating smaller chiral objects at nanoscale. Proceeding in this context, cross-stream migration in a viscoelastic medium has been utilized to focus two types of double-helical DNA molecules (radii of gyration $\sim O(0.1-1)\mu$m) in the vicinity of the centerline of a microchannel.[98] However, the throughput of this technique is limited due to its operational flow rate corresponding to $Re \sim O(10^{-3})$. By decreasing the size of the molecules, Brownian diffusive effects become significant which tend to destroy the focusing and alignment of separated objects. It will be interesting to seek new methods to remedy this problem and broaden the application of microfluidic techniques.

Even though trapping and ordering processes are well studied for non-motile cells, the interplay of cell motility with other hydrodynamic effects influencing the lateral migration is mostly overlooked. However in recent years, few studies have been conducted to shed light on the interaction between swimming behavior and shear flow. For example, Durham *et al.*[177] experimentally demonstrated the generation of intense accumulations of phytoplankton in the high-shear regions of confined flows due to tumbling behavior of the cells triggered by excessive hydrodynamic torque. In the microfluidic framework, Hashemi *et al.*[178] designed and fabricated a flow cytometer comprised of two sheath flows and a central sample stream in order to hydrodynamically focus and characterize various phytoplankton species. Also, Ardekani and Gore[179] have analytically shown that cross-stream migration induced by viscoelasticity can be used to aggregate bacterial cells in a vortical flow in order to generate large enough concentrations of microorganisms required for detection procedures. From practical point of view, detection of microorganisms such as bacteria is important in medical diagnosis and microbiological analysis of food, water, and environmental samples. Thus, another prominent area for future research can be towards providing insight upon the basic physics of lateral migration of motile cells in confined flows and its application in environmental and biological studies.

ACKNOWLEDGMENTS

[1]M. Danova, M. Torchio, and G. Mazzini, "Isolation of rare circulating tumor cells in cancer patients: Technical aspects and clinical implications," Expert Rev. Mol. Diagn. **11**, 473–485 (2011).

[2]D. C. Colter, I. Sekiya, and D. J. Prockop, "Identification of a subpopulation of rapidly self-renewing and multipotential adult stem cells in colonies of human marrow stromal cells," Proc. Natl. Acad. Sci. **98**, 7841–7845 (2001).

[3]K. Jo, Y.-L. Chen, J. J. de Pablo, and D. C. Schwartz, "Elongation and migration of single DNA molecules in microchannels using oscillatory shear flows," Lab Chip **9**, 2348–2355 (2009).

[4]P. Gascoyne, J. Satayavivad, and M. Ruchirawat, "Microfluidic approaches to malaria detection," Acta Tropica **89**, 357–369 (2004).

[5]A. van de Stolpe, K. Pantel, S. Sleijfer, L. W. Terstappen, and J. M. J. den Toonder, "Circulating tumor cell isolation and diagnostics: Toward routine clinical use," Cancer Res. **71**, 5955–5960 (2011).

[6]X. Cheng, D. Irimia, M. Dixon, K. Sekine, U. Demirci, L. Zamir, R. G. Tompkins, W. Rodriguez, and M. Toner, "A microfluidic device for practical label-free CD4+ T cell counting of HIV-infected subjects," Lab Chip **7**, 170–178 (2007).

[7]J. den Toonder, "Circulating tumor cells: The grand challenge," Lab Chip **11**, 375–377 (2011).

[8]D. Gänshirt, F. W. M. Smeets, A. Dohr, C. Walde, I. Steen, C. Lapucci, C. Falcinelli, R. Sant, M. Velasco, and H. S. P. Garritsen, "Enrichment of fetal nucleated red blood cells from the maternal circulation for prenatal diagnosis: Experiences with triple density gradient and MACS based on more than 600 cases," Fetal Diagn. Ther. **13**, 276–286 (1998).

[9]G. Vona, A. Sabile, M. Louha, V. Sitruk, S. Romana, K. Schütze, F. Capron, D. Franco, M. Pazzagli, M. Vekemans *et al*., "Isolation by size of epithelial tumor cells: A new method for the immunomorphological and molecular characterization of circulating tumor cells," Am. J. Pathol. **156**, 57–63 (2000).

[10]C. Alix-Panabières, J. Vendrell, O. Pellé, X. Rebillard, S. Riethdorf, V. Müller, M. Fabbro, and K. Pantel, "Detection and characterization of putative metastatic precursor cells in cancer patients," Clin. Chem. **53**, 537–539 (2007).

[11]H. M. Shapiro, *Practical Flow Cytometry*, 4th ed. (Wiley-Liss, New York, 2003).

[12]S. Miltenyi, W. Müller, W. Weichel, and A. Radbruch, "High gradient magnetic cell separation with MACS," Cytometry **11**, 231–238 (1990).

[13]A. A. S. Bhagat, H. Bow, H. W. Hou, S. J. Tan, J. Han, and C. T. Lim, "Microfluidics for cell separation," Med. Biol. Eng. Comput. **48**, 999–1014 (2010).

[14]A. H. J. Yang, S. D. Moore, B. S. Schmidt, M. Klug, M. Lipson, and D. Erickson, "Optical manipulation of nanoparticles and biomolecules in sub-wavelength slot waveguides," Nature (London) **457**, 71–75 (2009).

[15]A. E. Cohen, "Control of nanoparticles with arbitrary two-dimensional force fields," Phys. Rev. Lett. **94**, 118102 (2005).

[16]H. Lee, A. M. Purdon, and R. M. Westervelt, "Manipulation of biological cells using a microelectromagnet matrix," Appl. Phys. Lett. **85**, 1063–1065 (2004).

[17]M. Evander, L. Johansson, T. Lilliehorn, J. Piskur, M. Lindvall, S. Johansson, M. Almqvist, T. Laurell, and J. Nilsson, "Noninvasive acoustic cell trapping in a microfluidic perfusion system for online bioassays," Anal. Chem. **79**, 2984–2991 (2007).

[18]R. Dylla-Spears, J. E. Townsend, L. Jen-Jacobson, L. L. Sohn, and S. J. Muller, "Single-molecule sequence detection via microfluidic planar extensional flow at a stagnation point," Lab Chip **10**, 1543–1549 (2010).

[19]R. Pethig, "Review article—dielectrophoresis: Status of the theory, technology, and applications," Biomicrofluidics **4**, 022811 (2010).

[20]S. Patel, D. Showers, P. Vedantam, T. R. Tzeng, S. Qian, and X. Xuan, "Microfluidic separation of live and dead yeast cells using reservoir-based dielectrophoresis," Biomicrofluidics **6**, 034102 (2012).

[21]Z. Gagnon, J. Mazur, and H. C. Chang, "Glutaraldehyde enhanced dielectrophoretic yeast cell separation," Biomicrofluidics **3**, 044108 (2009).

[22]M. Muratore, V. Srsen, M. Waterfall, A. Downes, and R. Pethig, "Biomarker-free dielectrophoretic sorting of differentiating myoblast multipotent progenitor cells and their membrane analysis by Raman spectroscopy," Biomicrofluidics **6**, 034113 (2012).

[23]S. N. Murthy, "Magnetophoresis: An approach to enhance transdermal drug diffusion," Die Pharmazie **54**, 377 (1999).

[24]J. S. Heyman, "Acoustophoresis separation method," U.S. patent 5,192,450 (1993).

[25]M. P. MacDonald, G. C. Spalding, and K. Dholakia, "Microfluidic sorting in an optical lattice," Nature (London) **426**, 421–424 (2003).

[26]M. Yamada, M. Nakashima, and M. Seki, "Pinched flow fractionation: Continuous size separation of particles utilizing a laminar flow profile in a pinched microchannel," Anal. Chem. **76**, 5465–5471 (2004).

[27]T. A. Crowley and V. Pizziconi, "Isolation of plasma from whole blood using planar microfilters for lab-on-a-chip applications," Lab Chip **5**, 922–929 (2005).

[28]S. Yang, A. Ündar, and J. D. Zahn, "A microfluidic device for continuous, real time blood plasma separation," Lab Chip **6**, 871–880 (2006).

[29]S. Choi, S. Song, C. Choi, and J. K. Park, "Continuous blood cell separation by hydrophoretic filtration," Lab Chip **7**, 1532–1538 (2007).

[30]J. A. Davis, D. W. Inglis, K. J. Morton, D. A. Lawrence, L. R. Huang, S. Y. Chou, J. C. Sturm, and R. H. Austin, "Deterministic hydrodynamics: Taking blood apart," Proc. Natl. Acad. Sci. **103**, 14779–14784 (2006).

[31]J. Friend and L. Yeo, "Microscale acoustofluidics: Microfluidics driven via acoustics and ultrasonics," Rev. Mod. Phys. **83**, 647 (2011).

[32]A. Lenshof and T. Laurell, "Continuous separation of cells and particles in microfluidic systems," Chem. Soc. Rev. **39**, 1203–1217 (2010).

[33]X. Xuan, J. Zhu, and C. Church, "Particle focusing in microfluidic devices," Microfluid. Nanofluid. **9**, 1–16 (2010).

[34]D. R. Gossett, W. M. Weaver, A. J. Mach, S. C. Hur, H. T. K. Tse, W. Lee, H. Amini, and D. Di Carlo, "Label-free cell separation and sorting in microfluidic systems," Anal. Bioanal. Chem. **397**, 3249–3267 (2010).

[35]J. Chen, J. Li, and Y. Sun, "Microfluidic approaches for cancer cell detection, characterization, and separation," Lab Chip **12**, 1753–1767 (2012).

[36]J. Autebert, B. Coudert, F. C. Bidard, J. Y. Pierga, S. Descroix, L. Malaquin, and J. L. Viovy, "Microfluidic: An innovative tool for efficient cell sorting," Methods **57**, 297–307 (2012).

[37]H. Chang and G. Yossifon, "Understanding electrokinetics at the nanoscale: A perspective," Biomicrofluidics **3**, 012001 (2009).

[38]L. Y. Yeo and J. R. Friend, "Ultrafast microfluidics using surface acoustic waves," Biomicrofluidics **3**, 012002 (2009).

[39]J. Nilsson, M. Evander, B. Hammarstrom, and T. Laurell, "Review of cell and particle trapping in microfluidic systems," Anal. Chim. Acta **649**, 141–157 (2009).

[40]L. G. Leal, "Particle motions in a viscous fluid," Annu. Rev. Fluid Mech. **12**, 435–476 (1980).

[41]L. G. Leal, *Advanced Transport Phenomena: Fluid Mechanics and Convective Transport Processes* (Cambridge University Press, Cambridge, 2007).

[42]G. Segre, "Radial particle displacements in Poiseuille flow of suspensions," Nature (London) **189**, 209–210 (1961).

[43]G. Segre and A. Silberberg, "Behaviour of macroscopic rigid spheres in Poiseuille flow. Part 1. Determination of local concentration by statistical analysis of particle passages through crossed light beams," J. Fluid Mech. **14**, 115–135 (1962).

[44]G. Segre and A. Silberberg, "Behaviour of macroscopic rigid spheres in Poiseuille flow. Part 2. Experimental results and interpretation," J. Fluid Mech. **14**, 136–157 (1962).

[45]J. P. Matas, J. F. Morris, and E. Guazzelli, "Lateral forces on a sphere," Oil Gas Sci. Technol. **59**, 59–70 (2004).

[46]B. P. Ho and L. G. Leal, "Inertial migration of rigid spheres in two-dimensional unidirectional flows," J. Fluid Mech. **65**, 365–400 (1974).

[47]R. G. Cox and S. K. Hsu, "The lateral migration of solid particles in a laminar flow near a plane," Int. J. Multiphase Flow **3**, 201–222 (1977).

[48]J. A. Schonberg and E. J. Hinch, "Inertial migration of a sphere in Poiseuille flow," J. Fluid Mech. **203**, 517–524 (1989).

[49]A. J. Hogg, "The inertial migration of non-neutrally buoyant spherical particles in two-dimensional shear flows," J. Fluid Mech. **272**, 285–318 (1994).

[50]E. S. Asmolov, "The inertial lift on a spherical particle in a plane Poiseuille flow at large channel Reynolds number," J. Fluid Mech. **381**, 63–87 (1999).

[51]E. S. Asmolov, "The inertial lift on a small particle in a weak-shear parabolic flow," Phys. Fluids **14**, 15 (2002).

[52]J. S. Halow and G. B. Wills, "Radial migration of spherical particles in Couette systems," AIChE J. **16**, 281–286 (1970).

[53]J. P. Matas, J. F. Morris, and E. Guazzelli, "Inertial migration of rigid spherical particles in Poiseuille flow," J. Fluid Mech. **515**, 171–195 (2004).

[54]Y. S. Choi, K. W. Seo, and S. J. Lee, "Lateral and cross-lateral focusing of spherical particles in a square microchannel," Lab Chip **11**, 460–465 (2011).

[55]J. Feng, H. H. Hu, and D. D. Joseph, "Direct simulation of initial value problems for the motion of solid bodies in a Newtonian fluid. Part 2. Couette and Poiseuille flows," J. Fluid Mech. **277**, 271–301 (1994).

[56]L. Zeng, S. Balachandar, and P. Fischer, "Wall-induced forces on a rigid sphere at finite Reynolds number," J. Fluid Mech. **536**, 1–25 (2005).

[57]B. Chun and A. J. C. Ladd, "Inertial migration of neutrally buoyant particles in a square duct: An investigation of multiple equilibrium positions," Phys. Fluids **18**, 031704 (2006).

[58]D. Di Carlo, J. F. Edd, K. J. Humphry, H. A. Stone, and M. Toner, "Particle segregation and dynamics in confined flows," Phys. Rev. Lett. **102**, 94503 (2009).

[59]D. R. Gossett, H. T. K. Tse, J. S. Dudani, K. Goda, T. A. Woods, S. W. Graves, and D. Di Carlo, "Inertial manipulation and transfer of microparticles across laminar fluid streams," Small **8**, 2757–2764 (2012).

[60]A. A. S. Bhagat, H. W. Hou, L. D. Li, C. T. Lim, and J. Han, "Pinched flow coupled shear-modulated inertial microfluidics for high-throughput rare blood cell separation," Lab Chip **11**, 1870–1878 (2011).

[61]J. Oakey, R. W. Applegate, Jr., E. Arellano, D. D. Carlo, S. W. Graves, and M. Toner, "Particle focusing in staged inertial microfluidic devices for flow cytometry," Anal. Chem. **82**, 3862–3867 (2010).

[62]X. Mao, J. R. Waldeisen, and T. J. Huang, "'Microfluidic drifting'–Implementing three-dimensional hydrodynamic focusing with a single-layer planar microfluidic device," Lab Chip **7**, 1260–1262 (2007).

[63]D. Di Carlo, D. Irimia, R. G. Tompkins, and M. Toner, "Continuous inertial focusing, ordering, and separation of particles in microchannels," Proc. Natl. Acad. Sci. **104**, 18892–18897 (2007).

[64]S. C. Hur, H. T. K. Tse, and D. Di Carlo, "Sheathless inertial cell ordering for extreme throughput flow cytometry," Lab Chip **10**, 274–280 (2010).

[65]Z. Wu, B. Willing, J. Bjerketorp, J. K. Jansson, and K. Hjort, "Soft inertial microfluidics for high throughput separation of bacteria from human blood cells," Lab Chip **9**, 1193–1199 (2009).

[66]S. C. Hur, N. K. Henderson-MacLennan, E. R. B. McCabe, and D. Di Carlo, "Deformability-based cell classification and enrichment using inertial microfluidics," Lab Chip **11**, 912–920 (2011).

[67]S. S. Kuntaegowdanahalli, A. A. S. Bhagat, G. Kumar, and I. Papautsky, "Inertial microfluidics for continuous particle separation in spiral microchannels," Lab Chip **9**, 2973–2980 (2009).

[68]W. Lee, H. Amini, H. A. Stone, and D. Di Carlo, "Dynamic self-assembly and control of microfluidic particle crystals," Proc. Natl. Acad. Sci. **107**, 22413–22418 (2010).

[69]A. J. Mach and D. Di Carlo, "Continuous scalable blood filtration device using inertial microfluidics," Biotechnol. Bioeng. **107**, 302–311 (2010).

[70]D. Di Carlo, F. Jon, D. Irimia, R. G. Tompkins, and M. Toner, "Equilibrium separation and filtration of particles using differential inertial focusing," Anal. Chem. **80**, 2204–2211 (2008).

[71]A. A. S. Bhagat, S. S. Kuntaegowdanahalli, and I. Papautsky, "Inertial microfluidics for continuous particle filtration and extraction," Microfluid. Nanofluid. **7**, 217–226 (2009).

[72]S. C. Hur, A. J. Mach, and D. Di Carlo, "High-throughput size-based rare cell enrichment using microscale vortices," Biomicrofluidics **5**, 022206 (2011).

[73]D. Di Carlo, "Inertial microfluidics," Lab Chip **9**, 3038–3046 (2009).

[74]J. Takagi, M. Yamada, M. Yasuda, and M. Seki, "Continuous particle separation in a microchannel having asymmetrically arranged multiple branches," Lab Chip **5**, 778–784 (2005).

[75]M. Yamada and M. Seki, "Hydrodynamic filtration for on-chip particle concentration and classification utilizing microfluidics," Lab Chip **5**, 1233–1239 (2005).

[76]L. R. Huang, E. C. Cox, R. H. Austin, and J. C. Sturm, "Continuous particle separation through deterministic lateral displacement," Science **304**, 987–990 (2004).

[77]D. W. Inglis, J. A. Davis, R. H. Austin, and J. C. Sturm, "Critical particle size for fractionation by deterministic lateral displacement," Lab Chip **6**, 655–658 (2006).

[78]B. R. Long, M. Heller, J. P. Beech, H. Linke, H. Bruus, and J. O. Tegenfeldt, "Multidirectional sorting modes in deterministic lateral displacement devices," Phys. Rev. E **78**, 046304 (2008).

[79]S. Choi and J. K. Park, "Continuous hydrophoretic separation and sizing of microparticles using slanted obstacles in a microchannel," Lab Chip **7**, 890–897 (2007).

[80]S. Choi, S. Song, C. Choi, and J. K. Park, "Microfluidic self-sorting of mammalian cells to achieve cell cycle synchrony by hydrophoresis," Anal. Chem. **81**, 1964–1968 (2009).

[81]J. S. Park, S. H. Song, and H. I. Jung, "Continuous focusing of microparticles using inertial lift force and vorticity via multi-orifice microfluidic channels," Lab Chip **9**, 939–948 (2009).

[82]J. S. Park and H. I. Jung, "Multiorifice flow fractionation: Continuous size-based separation of microspheres using a series of contraction/expansion microchannels," Anal. Chem. **81**, 8280–8288 (2009).

[83]A. Karnis and S. G. Mason, "Particle motions in sheared suspensions. XIX. Viscoelastic media," Trans. Soc. Rheol. **10**, 571–592 (1966).

[84]F. Gauthier, H. L. Goldsmith, and S. G. Mason, "Particle motions in non-Newtonian media. II. Poiseuille flow," Trans. Soc. Rheol. **15**, 297–330 (1971).

[85]E. Bartram, H. L. Goldsmith, and S. G. Mason, "Particle motions in non-Newtonian media," Rheol. Acta **14**, 776–782 (1975).

[86]M. A. Tehrani, "An experimental study of particle migration in pipe flow of viscoelastic fluids," J. Rheol. **40**, 1057–1077 (1996).

[87]B. P. Ho and L. G. Leal, "Migration of rigid spheres in a two-dimensional unidirectional shear flow of a second-order fluid," J. Fluid Mech. **76**, 783 (1976).

[88]P. Y. Huang, J. Feng, H. H. Hu, and D. D. Joseph, "Direct simulation of the motion of solid particles in Couette and Poiseuille flows of viscoelastic fluids," J. Fluid Mech. **343**, 73–94 (1997).

[89]A. M. Ardekani, R. H. Rangel, and D. D. Joseph, "Motion of a sphere normal to a wall in a second-order fluid," J. Fluid Mech. **587**, 163–172 (2007).

[90]A. M. Ardekani, R. H. Rangel, and D. D. Joseph, "Two spheres in a free stream of a second-order fluid," Phys. Fluids **20**, 063101 (2008).

[91]S. A. Dhahir and K. Walters, "On non-Newtonian flow past a cylinder in a confined flow," J. Rheol. **33**, 781–804 (1989).

[92]P. Y. Huang and D. D. Joseph, "Effects of shear thinning on migration of neutrally buoyant particles in pressure driven flow of Newtonian and viscoelastic fluids," J. Non-Newtonian Fluid Mech. **90**, 159–185 (2000).

[93]R. B. Bird, R. C. Armstrong, and O. Hassager, *Dynamics of Polymeric Liquids: Fluid Mechanics* (John Wiley and Sons, Inc., New York, NY, 1987), Vol. 1.

[94]A. M. Leshansky, A. Bransky, N. Korin, and U. Dinnar, "Tunable nonlinear viscoelastic "focusing" in a microfluidic device," Phys. Rev. Lett. **98**, 234501 (2007).

[95]S. Yang, S. S. Lee, S. W. Ahn, K. Kang, W. Shim, G. Lee, K. Hyun, and J. M. Kim, "Deformability-selective particle entrainment and separation in a rectangular microchannel using medium viscoelasticity," Soft Matter **8**, 5011–5019 (2012).

[96]G. D'Avino, P. L. Maffettone, F. Greco, and M. A. Hulsen, "Viscoelasticity-induced migration of a rigid sphere in confined shear flow," J. Non-Newtonian Fluid Mech. **165**, 466–474 (2010).

[97]G. D'Avino, G. Romeo, M. M. Villone, F. Greco, P. A. Netti, and P. L. Maffettone, "Single line particle focusing induced by viscoelasticity of the suspending liquid: Theory, experiments and simulations to design a micropipe flow-focuser," Lab Chip **12**, 1638–1645 (2012).

[98]J. Y. Kim, S. W. Ahn, S. S. Lee, and J. M. Kim, "Lateral migration and focusing of colloidal particles and DNA molecules under viscoelastic flow," Lab Chip **12**, 2807–2814 (2012).

[99]S. Yang, J. Y. Kim, S. J. Lee, S. S. Lee, and J. M. Kim, "Sheathless elasto-inertial particle focusing and continuous separation in a straight rectangular microchannel," Lab Chip **11**, 266–273 (2011).

[100]J. Nam, H. Lim, D. Kim, H. Jung, and S. Shin, "Continuous separation of microparticles in a microfluidic channel via the elasto-inertial effect of non-Newtonian fluid," Lab Chip **12**, 1347–1354 (2012).

[101]A. M. Dondorp, P. A. Kager, J. Vreeken, and N. J. White, "Abnormal blood flow and red blood cell deformability in severe malaria," Parasitol. Today **16**, 228–232 (2000).

[102]F. C. Mokken, M. Kedaria, C. P. Henny, M. R. Hardeman, and A. W. Gelb, "The clinical importance of erythrocyte deformability, a hemorrheological parameter," Ann. Hematol. **64**, 113–122 (1992).

[103]S. E. Cross, Y. S. Jin, J. Rao, and J. K. Gimzewski, "Nanomechanical analysis of cells from cancer patients," Nat. Nanotechnol. **2**, 780–783 (2007).

[104]S. Suresh, "Biomechanics and biophysics of cancer cells," Acta Mater. **55**, 3989–4014 (2007).

[105]S. K. Ballas, "Sickle cell anemia with few painful crises is characterized by decreased red cell deformability and increased number of dense cells," Am. J. Hematol. **36**, 122–130 (2006).

[106]P. C. H. Chan and L. G. Leal, "The motion of a deformable drop in a second-order fluid," J. Fluid Mech. **92**, 131–170 (1979).

[107]F. Takemura, S. Takagi, J. Magnaudet, and Y. Matsumoto, "Drag and lift forces on a bubble rising near a vertical wall in a viscous liquid," J. Fluid Mech. **461**, 277–300 (2002).

[108]F. Takemura and J. Magnaudet, "The transverse force on clean and contaminated bubbles rising near a vertical wall at moderate Reynolds number," J. Fluid Mech. **495**, 235–253 (2003).

[109]J. Magnaudet, S. Takagi, and D. Legendre, "Drag, deformation and lateral migration of a buoyant drop moving near a wall," J. Fluid Mech. **476**, 115–157 (2003).

[110]S. K. Doddi and P. Bagchi, "Lateral migration of a capsule in a plane Poiseuille flow in a channel," Int. J. Multiphase Flow **34**, 966–986 (2008).

[111]S. Mortazavi and G. Tryggvason, "A numerical study of the motion of drops in Poiseuille flow. Part 1. Lateral migration of one drop," J. Fluid Mech. **411**, 325–350 (2000).

[112]B. Lorz, R. Simson, J. Nardi, and E. Sackmann, "Weakly adhering vesicles in shear flow: Tanktreading and anomalous lift force," Europhys. Lett. **51**, 468 (2000).

[113]S. Sukumaran and U. Seifert, "Influence of shear flow on vesicles near a wall: A numerical study," Phys. Rev. E **64**, 011916 (2001).

[114]W. S. J. Uijttewaal, E. J. Nijhof, and R. M. Heethaar, "Droplet migration, deformation, and orientation in the presence of a plane wall: A numerical study compared with analytical theories," Phys. Fluids A: Fluid Dyn. **5**, 819–825 (1993).

[115]G. Coupier, B. Kaoui, T. Podgorski, and C. Misbah, "Noninertial lateral migration of vesicles in bounded Poiseuille flow," Phys. Fluids **20**, 111702 (2008).

[116]M. Abkarian and A. Viallat, "Dynamics of vesicles in a wall-bounded shear flow," Biophys. J. **89**, 1055–1066 (2005).

[117]M. Abkarian and A. Viallat, "Vesicles and red blood cells in shear flow," Soft Matter **4**, 653–657 (2008).

[118]U. Seifert, K. Berndl, and R. Lipowsky, "Shape transformations of vesicles: Phase diagram for spontaneous-curvature and bilayer-coupling models," Phys. Rev. A **44**, 1182 (1991).

[119]P. M. Vlahovska and R. S. Gracia, "Dynamics of a viscous vesicle in linear flows," Phys. Rev. E **75**, 016313 (2007).

[120]P. M. Vlahovska, T. Podgorski, and C. Misbah, "Vesicles and red blood cells in flow: From individual dynamics to rheology," C. R. Phys. **10**, 775–789 (2009).

[121]A. J. Griggs, A. Z. Zinchenko, and R. H. Davis, "Low-Reynolds-number motion of a deformable drop between two parallel plane walls," Int. J. Multiphase Flow **33**, 182–206 (2007).

[122]B. Alberts, *Molecular Biology of the Cell*, 4th ed. (Garland Science, New York, 2002).

[123]R. Dimova, K. A. Riske, S. Aranda, N. Bezlyepkina, R. L. Knorr, and R. Lipowsky, "Giant vesicles in electric fields," Soft Matter **3**, 817–827 (2007).

[124]S. R. Keller and R. Skalak, "Motion of a tank-treading ellipsoidal particle in a shear flow," J. Fluid Mech. **120**, 27–47 (1982).

[125]P. Olla, "The lift on a tank-treading ellipsoidal cell in a shear flow," J. Phys. II **7**, 1533–1540 (1997).

[126]G. Danker, P. M. Vlahovska, and C. Misbah, "Vesicles in Poiseuille flow," Phys. Rev. Lett. **102**, 148102 (2009).

[127]B. Kaoui, G. H. Ristow, I. Cantat, C. Misbah, and W. Zimmermann, "Lateral migration of a two-dimensional vesicle in unbounded Poiseuille flow," Phys. Rev. E **77**, 021903 (2008).

[128]T. M. Geislinger, B. Eggart, S. Braunmuller, L. Schmid, and T. Franke, "Separation of blood cells using hydrodynamic lift," Appl. Phys. Lett. **100**, 183701 (2012).

[129]W. R. Dean, "Fluid motion in a curved channel," Proc. R. Soc. London, Ser. A **121**, 402–420 (1928).

[130]S. A. Berger, L. Talbot, and L. S. Yao, "Flow in curved pipes," Annu. Rev. Fluid Mech. **15**, 461–512 (1983).

[131]S. Ookawara, R. Higashi, D. Street, and K. Ogawa, "Feasibility study on concentration of slurry and classification of contained particles by microchannel," Chem. Eng. J. **101**, 171–178 (2004).

[132]T. M. Squires and S. R. Quake, "Microfluidics: Fluid physics at the nanoliter scale," Rev. Modern Phys. **77**, 977 (2005).

[133]D. R. Gossett and D. Di Carlo, "Particle focusing mechanisms in curving confined flows," Anal. Chem. **81**, 8459–8465 (2009).

[134]X. Mao, S. C. S. Lin, C. Dong, and T. J. Huang, "Single-layer planar on-chip flow cytometer using microfluidic drifting based three-dimensional (3D) hydrodynamic focusing," Lab Chip **9**, 1583–1589 (2009).

[135]A. A. S. Bhagat, S. S. Kuntaegowdanahalli, and I. Papautsky, "Continuous particle separation in spiral microchannels using Dean flows and differential migration," Lab Chip **8**, 1906–1914 (2008).

[136]A. A. S. Bhagat, S. S. Kuntaegowdanahalli, N. Kaval, C. J. Seliskar, and I. Papautsky, "Inertial microfluidics for sheathless high-throughput flow cytometry," Biomed. Microdevices **12**, 187–195 (2010).

[137]J. Wang, Y. Zhan, V. M. Ugaz, and C. Lu, "Vortex-assisted DNA delivery," Lab Chip **10**, 2057–2061 (2010).

[138]J. Zhu and X. Xuan, "Curvature-induced dielectrophoresis for continuous separation of particles by charge in spiral microchannels," Biomicrofluidics **5**, 024111 (2011).

[139]E. W. M. Kemna, R. M. Schoeman, F. Wolbers, I. Vermes, D. A. Weitz, and A. van den Berg, "High-yield cell ordering and deterministic cell-in-droplet encapsulation using Dean flow in a curved microchannel," Lab Chip **12**, 2881–2887 (2012).

[140]C. Church, J. Zhu, G. Wang, T. R. J. Tzeng, and X. Xuan, "Electrokinetic focusing and filtration of cells in a serpentine microchannel," Biomicrofluidics **3**, 044109 (2009).

[141]W. C. Lee, A. A. S. Bhagat, S. Huang, K. J. Van Vliet, J. Han, and C. T. Lim, "High-throughput cell cycle synchronization using inertial forces in spiral microchannels," Lab Chip **11**, 1359–1367 (2011).

[142]C. M. Lin, Y. S. Lai, H. P. Liu, C. Y. Chen, and A. M. Wo, "Trapping of bioparticles via microvortices in a microfluidic device for bioassay applications," Anal. Chem. **80**, 8937–8945 (2008).

[143]H. M. Hertz, "Standing-wave acoustic trap for nonintrusive positioning of microparticles," J. Appl. Phys. **78**, 4845–4849 (1995).

[144]T. M. Squires and M. Z. Bazant, "Induced-charge electro-osmosis," J. Fluid Mech. **509**, 217–252 (2004).

[145]A. Gonzalez, A. Ramos, N. G. Green, A. Castellanos, and H. Morgan, "Fluid flow induced by nonuniform ac electric fields in electrolytes on microelectrodes. II. A linear double-layer analysis," Phys. Rev. E **61**, 4019–4028 (2000).

[146]L. Y. Yeo, D. Hou, S. Maheshswari, and H. Chang, "Electrohydrodynamic surface microvortices for mixing and particle trapping," Appl. Phys. Lett. **88**, 233512 (2006).

[147]D. Hou, S. Maheshwari, and H. Chang, "Rapid bioparticle concentration and detection by combining a discharge driven vortex with surface enhanced Raman scattering," Biomicrofluidics **1**, 014106 (2007).

[148]S. Liu, H. Wei, S. Hwang, and H. Chang, "Dynamic particle trapping, release, and sorting by microvortices on a sub-strate," Phys. Rev. E **82**, 026308 (2010).

[149]D. Ahmed, X. Mao, J. Shi, B. K. Juluri, and T. J. Huang, "A millisecond micromixer via single-bubble-based acoustic streaming," Lab Chip **9**, 2738–2741 (2009).

[150]D. Ahmed, X. Mao, B. K. Juluri, and T. J. Huang, "A fast microfluidic mixer based on acoustically driven sidewall-trapped microbubbles," Microfluid. Nanofluid. **7**, 727–731 (2009).

[151]R. H. Liu, J. Yang, M. Z. Pindera, M. Athavale, and P. Grodzinski, "Bubble-induced acoustic micromixing," Lab Chip **2**, 151–157 (2002).

[152]A. R. Tovar and A. P. Lee, "Lateral cavity acoustic transducer," Lab Chip **9**, 41–43 (2009).

[153]K. Ryu, S. K. Chung, and S. K. Cho, "Micropumping by an acoustically excited oscillating bubble for automated implantable microfluidic devices," J. Assoc. Lab Autom. **15**, 163–171 (2010).

[154]Y. Xie, D. Ahmed, M. I. Lapsley, S. C. S. Lin, A. A. Nawaz, L. Wang, and T. J. Huang, "Single-shot characterization of enzymatic reaction constants K_m and k_{cat} by an acoustic-driven, bubble-based fast micromixer," Anal. Chem. **84**(17), 7495–7501 (2012).

[155]P. Marmottant and S. Hilgenfeldt, "Controlled vesicle deformation and lysis by single oscillating bubbles," Nature (London) **423**, 153–156 (2003).

[156]C. Wang, S. V. Jalikop, and S. Hilgenfeldt, "Size-sensitive sorting of microparticles through control of flow geometry," Appl. Phys. Lett. **99**, 034101 (2011).

[157]C. Wang, S. V. Jalikop, and S. Hilgenfeldt, "Efficient manipulation of microparticles in bubble streaming flows," Biomicrofluidics **6**, 012801 (2012).

[158]A. Hashmi, G. Yu, M. Reilly-Collette, G. Heiman, and J. Xu, "Oscillating bubbles: A versatile tool for lab on a chip applications," Lab Chip **12**, 4216–4227 (2012).

[159]M. Prakash and N. Gershenfeld, "Microfluidic bubble logic," Science **315**, 832–835 (2007).

[160]J. S. Raut, S. D. Stoyanov, C. Duggal, E. G. Pelan, L. N. Arnaudov, and V. M. Naik, "Hydrodynamic cavitation: A bottom-up approach to liquid aeration," Soft Matter **8**, 4562–4566 (2012).

[161]P. Dawson, "The physics of the oscillating bubble made simple," Eur. J. Radiol. **41**, 176–178 (2002).

[162]W. L. Nyborg, *Acoustic Streaming* (Academic Press, New York, 1965), Vol. 2.

[163]N. Riley, "Steady streaming," Annu. Rev. Fluid Mech. **33**, 43–65 (2001).

[164]D. L. Miller and E. A. Neppiras, "On the oscillation mode of gas-filled micropores," J. Acoust. Soc. Am. **77**, 946 (1985).

[165]C. Pozrikidis, *Boundary Integral and Singularity Methods for Linearized Viscous Flow* (Cambridge University Press, Cambridge, 1992), Vol. 7.

[166]M. Z. Bazant, "Induced-charge electrokinetic phenomena," in *Electrokinetics and Electrohydrodynamics in Microsystems* (CISM, 2011), pp. 221–297.

[167]K. V. Sharp, S. H. Yazdi, and S. M. Davison, "Localized flow control in microchannels using induced-charge electroos-mosis near conductive obstacles," Microfluid. Nanofluid. **10**, 1257–1267 (2011).

[168]J. A. Levitan, S. Devasenathipathy, V. Studer, Y. Ben, T. Thorsen, T. M. Squires, and M. Z. Bazant, "Experimental ob-servation of induced-charge electro-osmosis around a metal wire in a microchannel," Colloids Surf., A **267**, 122–132 (2005).

[169]S. H. Yazdi and A. M. Ardekani, "Bacterial aggregation and biofilm formation in a vortical flow," Biomicrofluidics **6**, 044114 (2012).

[170]B. R. Lutz, J. Chen, and D. T. Schwartz, "Microscopic steady streaming eddies created around short cylinders in a chan-nel: Flow visualization and stokes layer scaling," Phys. Fluids **17**, 023601 (2005).

[171]B. R. Lutz, J. Chen, and D. T. Schwartz, "Hydrodynamic tweezers: 1. Noncontact trapping of single cells using steady streaming microeddies," Anal. Chem. **78**, 5429–5435 (2006).

[172]V. H. Lieu, T. A. House, and D. T. Schwartz, "Hydrodynamic tweezers: Impact of design geometry on flow and micro-particle trapping," Anal. Chem. **84**, 1963–1968 (2012).

[173]S. Ahuja, *Chiral Separations: Applications and Technology* (American Chemical Society, Washington, DC, 1997).

[174]P. Chen and C. H. Chao, "Lift forces of screws in shear flows," Phys. Fluids **19**, 017108 (2007).

[175]M. Makino, L. Arai, and M. Doi, "Shear migration of chiral particle in parallel-disk," J. Phys. Soc. Jpn. **77**, 064404 (2008).

[176]Marcos, H. C. Fu, T. R. Powers, and R. Stocker, "Separation of microscale chiral objects by shear flow," Phys. Rev. Lett. **102**, 158103 (2009).

[177]W. M. Durham, J. O. Kessler, and R. Stocker, "Disruption of vertical motility by shear triggers formation of thin phyto-plankton layers," Science **323**, 1067–1070 (2009).

[178]N. Hashemi, J. S. Erickson, J. P. Golden, and F. S. Ligler, "Optofluidic characterization of marine algae using a micro-flow cytometer," Biomicrofluidics **5**, 032009 (2011).

[179]A. M. Ardekani and E. Gore, "Emergence of a limit cycle for swimming microorganisms in a vortical flow of a visco-elastic fluid," Phys. Rev. E **85**, 056309 (2012).